

ORIGINAL ARTICLE

Open Access



Behavior of FRP-Strengthened RC Beams with Large Rectangular Web Openings in Flexure Zones: Experimental and Numerical Study

Tarek Almusallam, Yousef Al-Salloum*, Hussein Elsanadedy, Abdulhafiz Alshenawy and Rizwan Iqbal

Abstract

This paper aims to investigate the behavior of fiber reinforced polymer (FRP) strengthened reinforced concrete (RC) beams containing large rectangular web openings in the flexure zone. Studied parameters were type of loading, opening size and strengthening scheme. Seven RC beams categorized into two different groups were tested. In the first group, two unstrengthened beams (one solid without opening and one with large rectangular web opening in the pure flexure zone) were tested under four-point bending. In the second group, five beams were tested under center-point loading. They comprised of one reference solid beam and four beams with large rectangular web opening in the maximum-moment region. Out of the four beams with openings, two specimens were unstrengthened and the other two were strengthened with two different FRP schemes. A numerical study was also conducted and the results of analysis were validated with experiments. The calibrated analysis was then used for some useful parametric studies in which the effect of different parameters was investigated.

Keywords: RC beams, openings, flexural strengthening, FRP, steel plates, FE modeling

1 Introduction

The web openings in reinforced concrete (RC) beams are frequently used for passing utility ducts and pipes. These openings accommodate vital building services that may include electricity, air conditioning, water supply, computer and telecommunication network. The web openings in RC beams may be of different shapes such as rectangular, circular, trapezoidal, diamond, and many other shapes. The rectangular and circular shapes are the more prevalent shapes in practice (Prentzas 1968). Web openings can be located in either high shear zones such as areas close to the column support in RC beams or high flexure zones such as areas near mid-span of beams. Examples of rectangular web opening in flexure zone of simply supported RC beams are given in Fig. 1. Many

researchers have used the terms “small” and “large” openings for their classification without any clear distinction. Mansur (1998) suggested the criteria to classify the size of openings. Author classified the web opening as small if $\ell_o \leq h_c$ where ℓ_o is the length of the opening and h_c is the larger of h_b and h_t ; where h_b and h_t are the depths of bottom and top chords, respectively (see Fig. 1). For large opening, $\ell_o > h_c$.

The post-construction creation of an opening in the web of RC beams reduces the web cross-section and consequently reduces the flexural stiffness and shear capacity and increases the beam deflection at service load (Tan et al. 1996; Mansur 1998; Mansur et al. 1999). In case an opening in the RC beam is planned at design stage, additional rebars can be installed around the web opening for making up for the loss in strength and stiffness. For post-constructed openings in the existing RC beams, retrofitting of beams is needed. Fiber reinforced polymer (FRP) laminates are widely popular in building construction for the strengthening of structural members (Kachlakev and

*Correspondence: ysalloum@ksu.edu.sa

Chair of Research and Studies in Strengthening and Rehabilitation of Structures, Department of Civil Engineering, College of Engineering, King Saud University, P.O. Box 800, Riyadh 11421, Saudi Arabia
Journal information: ISSN 1976-0485 / eISSN 2234-1315

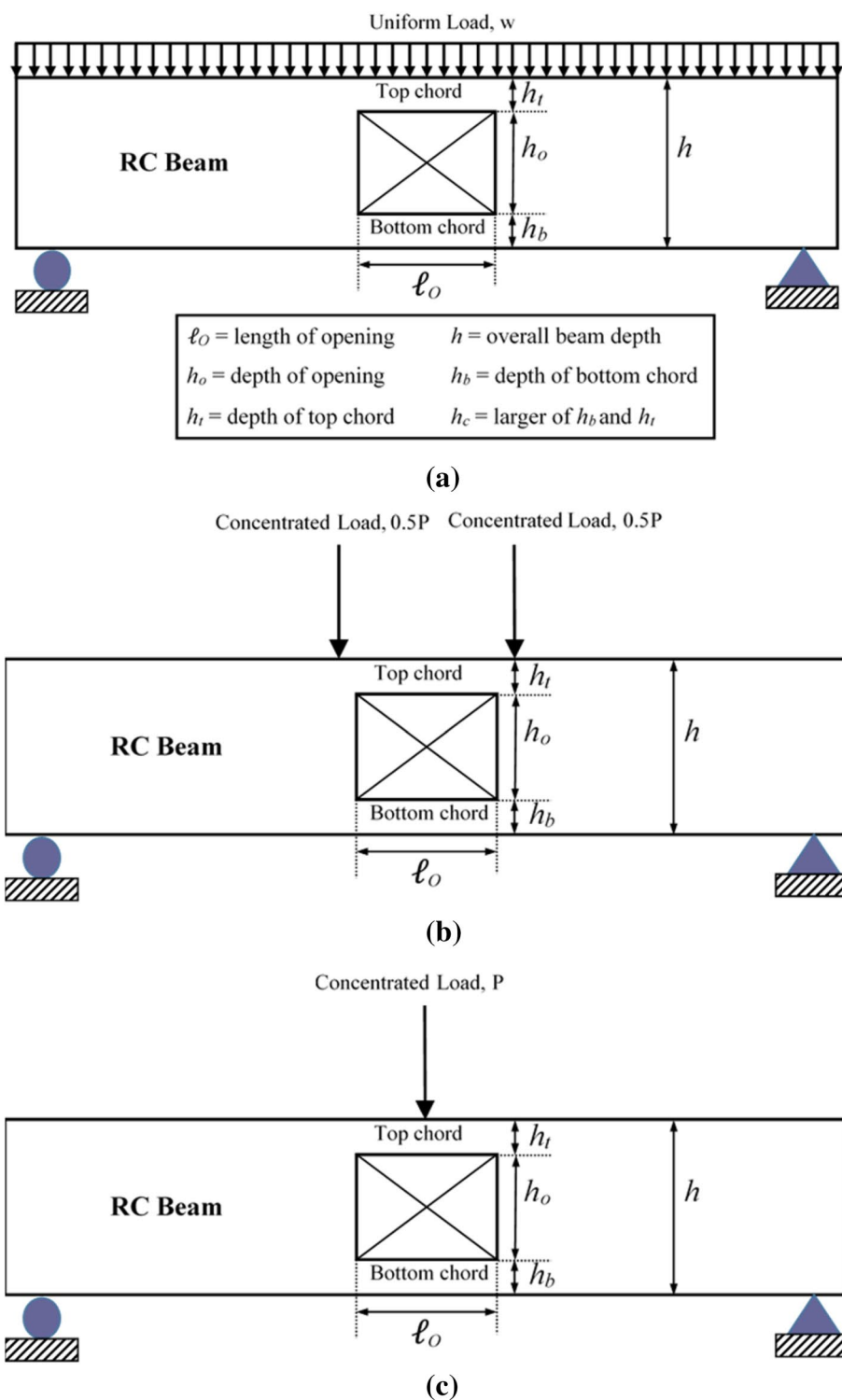


Fig. 1 Rectangular web opening in flexure zone of a simply supported RC beam: **a** opening in zone of high flexure with low shear (case of uniform load), **b** opening in zone of pure flexure with zero shear (case of 4-point bending), and **c** opening in zone of high flexure with high shear (case of center-point loading).

McCurry 2000; Al-Salloum 2007; Alsayed et al. 2010; Al-Salloum et al. 2011; Elsanadedy et al. 2012a, b; Alsayed et al. 2014; Elsanadedy et al. 2015, 2016; Shehab et al. 2017). The influence of FRP laminates on the response of solid RC beams under flexure (Alagusundaramoorthy et al. 2003; Ashour et al. 2004; Hawileh et al. 2013) and shear (Li et al. 2001; Zhang et al. 2004; Islam et al. 2005) has been widely studied. However, the research on the use of FRP laminates in the strengthening of RC beams with opening is limited (Mansur et al. 1999; Abdalla et al. 2003; El Maaddawy and Sherif 2009; Pimanmas 2010; Chin et al. 2011; Hawileh et al. 2012; Nie et al. 2018). The studies were performed using experiments (Mansur et al. 1999; Abdalla et al. 2003; El Maaddawy and Sherif 2009; Pimanmas 2010; Chin et al. 2011; Nie et al. 2018) and validated with nonlinear finite element (FE) analysis (Pimanmas 2010; Hawileh et al. 2012). Some of these studies are briefly described below.

Mansur et al. (1999) tested nine RC T-beams having circular openings. The beams were strengthened using FRP plates, which were applied around the opening in the form of a truss. For avoiding premature debonding failure, the FRP plates were anchored to RC beam using expansion bolts. The test results demonstrated the effectiveness of FRP strengthening in improving the response of the existing RC beams with openings.

El Maaddawy and Sherif (2009) examined the role of externally bonded CFRP laminates in strengthening RC deep beams with web openings. Thirteen deep beams with two square web openings, symmetrically located in each shear span, were tested in flexure up to failure. The effect of the location and size of openings were studied. The CFRP strengthening was found to be quite effective in enhancing the shear capacity of the deep beams. Analytical models were also developed to predict the shear capacity of the FRP-upgraded RC deep beams with openings.

Chin et al. (2011) studied experimentally the performance of CFRP-strengthened RC beams having square and circular openings in flexure zone. Five beams were tested in flexure up to failure. It was reported that large opening in flexure zone increases cracking and deflection and reduces the load capacity and stiffness. A strengthening configuration was designed for each unstrengthened beam based on their respective crack patterns. CFRP laminates remarkably restored the original capacity of the beam with the large circular opening in flexure zone, while 10% regain of beam capacity was achieved for the beam with the square opening.

Hawileh et al. (2012) developed 3D nonlinear FE models to predict the behavior of RC deep beams containing web openings and strengthened in shear with CFRP composites. The web openings partially or fully interrupted

the natural load path. In the FE models, 8-node solid and 2-node link elements were used to represent concrete volume and steel rebars, respectively, whereas, multi-layer shell elements were employed to simulate the CFRP sheets. In addition to material nonlinearity, special interface elements were implemented in the models to simulate the interfacial bond behavior between concrete and CFRP composites. A comparison between the FE results and experimental data published in the literature demonstrated the validity of the computational models in capturing the structural response for both unstrengthened and CFRP-strengthened deep beams with openings.

In a more recent study, Nie et al. (2018) tested eight full-scale RC beams under center-point loading up to failure. Two specimens (one with rectangular section and one with T-section) were solid without openings and the other six beams were constructed with T-section and contained single rectangular web opening in shear zone. Out of the six T-beams with openings, two specimens were unstrengthened and six beams were strengthened with externally bonded CFRP composite sheets. Test results showed that a sizable web opening can effectively reduce the flexural capacity of the T-beam and the CFRP strengthening system is needed to avoid shear failure of the beam and confine the web chord created by the opening to ensure a ductile response.

Even though some studies have been published on FRP-upgraded RC beams with web openings located in shear zones, research on FRP-graded RC beams with web openings in flexure zones is very limited. This highlights the need for more research in this area. The goal of this study is to examine experimentally and numerically the influence of large rectangular web opening in the flexure zone on the response of unstrengthened and strengthened RC beams. Studied parameters included type of loading, opening size and strengthening scheme. Seven RC beams were prepared and tested up to failure. Two loading types, two different opening sizes as well as two different strengthening schemes were investigated. In addition to the experimental program, nonlinear FE analysis was carried out using LS-DYNA software (2007). The validated numerical analysis was then used for some useful parametric studies in which the effect of different parameters such as opening size and strengthening schemes was studied.

2 Experimental Program

2.1 Test Matrix

The test program comprised of seven RC beams with section dimensions of 200×450 mm. Details of the experimental program are presented in Table 1. Beams were categorized into two different groups. In the first group, two unstrengthened beams were tested under four-point

Table 1 Test matrix.

Beam ID	Opening size (mm)		Type of loading	Strengthening scheme	No. of specimens	Notes
	Depth, h_o	Length, ℓ_o				
BC-N-4PB	No opening		4-point bending	Unstrengthened	1	Control specimen
BC-O1-4PB	225	450	4-point bending	Unstrengthened	1	Control specimen
BC-N-CPL	No opening		Center-point loading	Unstrengthened	1	Control specimen
BC-O1-CPL	225	450	Center-point loading	Unstrengthened	1	Control specimen
BS1-O1-CPL	225	450	Center-point loading	Strengthened with scheme-1: 2 layers ($0^\circ/90^\circ$) of carbon/epoxy system (see Fig. 4)	1	
BC-O2-CPL	225	900	Center-point loading	Unstrengthened	1	Control specimen
BS2-O2-CPL	225	900	Center-point loading	Strengthened with scheme-2: 2 layers ($0^\circ/90^\circ$) of E-glass/epoxy system + 5 mm thick steel plates (see Fig. 6)	1	
Total no. of specimens					7	

bending (4PB). They included one reference specimen without opening (i.e., solid beam) and the other beam was constructed with a large rectangular web opening of 225 mm depth and 450 mm length in the pure flexure zone. In the second group, five beams were tested under center-point loading (CPL). They comprised of one reference solid beam, two beams with mid-span rectangular opening of 225 mm depth and 450 mm length and two beams with mid-span rectangular opening of 225 mm depth and 900 mm length (see Table 1). Out of the four beams with openings, two specimens were unstrengthened and the other two were strengthened with two different schemes. The beam with 450 mm opening was strengthened using two layers ($0^\circ/90^\circ$) of externally bonded CFRP sheets (scheme-1). However, the beam with 900 mm opening was upgraded with scheme-2, which is a hybrid system comprising of externally bonded glass fiber reinforced polymer (GFRP) sheets anchored with bolted steel plates located above the opening.

2.2 Test Specimen Details and Preparation

Details of unstrengthened specimens are given in Figs. 2 and 3 for beams with 4-point bending and center-point loading, respectively. The arrangement of reinforcement for all the beams consists of 3 ϕ 16 mm rebars as longitudinal tension steel and 2 ϕ 10 mm rebars as compression reinforcement. Stirrups of ϕ 8 mm @ 150 mm c/c spacing were provided as transverse reinforcement. For beams with openings, a single rectangular opening was constructed at mid-span and it was located symmetrically, as shown in Figs. 2 and 3. For beams BC-O1-4PB, BC-O1-CPL and BS1-O1-CPL, the opening had a length of 450 mm and a depth of 225 mm. However, for beams BC-O2-CPL and BS2-O2-CPL, the opening length was increased to 900 mm. As seen in Figs. 2 and 3, U-stirrups

were provided in the bottom and top chords of the opening, thus representing the creation of the opening on site by cutting concrete and steel stirrups in existing beams.

The strengthening schemes were designed once the flexural tests for the unstrengthened specimens with and without openings were done and the failure patterns established. As mentioned earlier, two different schemes were designed in this study. The first scheme (scheme-1) involved the use of CFRP laminates and the second scheme (scheme-2) involved the use of GFRP laminates anchored using steel plates. Details of beam strengthened with scheme-1 (BS1-O1-CPL) are given in Fig. 4. In addition, steps involved in strengthening of beam BS1-O1-CPL using scheme-1 are depicted in Fig. 5. As shown in Figs. 4 and 5, the first scheme comprised of applying two layers of CFRP sheets in the designated patterns. CFRP strips of 112.5 mm width were applied to the bottom and top chords of the beam first, with the primary fibers oriented longitudinally. The length of these strips was 900 mm, as shown in Fig. 4a. The strips were applied on both sides of RC beams. On top of these strips, the second layer of CFRP was applied with the pattern shown in Fig. 4b. The second layer comprised of four pieces of CFRP sheets with fibers oriented vertically, which were applied separately to the top and bottom chords, and on both sides of the opening. It should be noted that the chord above the opening and the two sides were wrapped using a U-shape wrap; whereas, the chord below the opening was fully wrapped. The reason for this being that practically it would not be possible to wrap the top chord fully due to the presence of slab on top of the beam.

The second scheme of strengthening (scheme-2) comprised of GFRP sheets in combination with steel plates. The purpose of using steel plates was to make sure the GFRP sheet was properly anchored to the beam and at

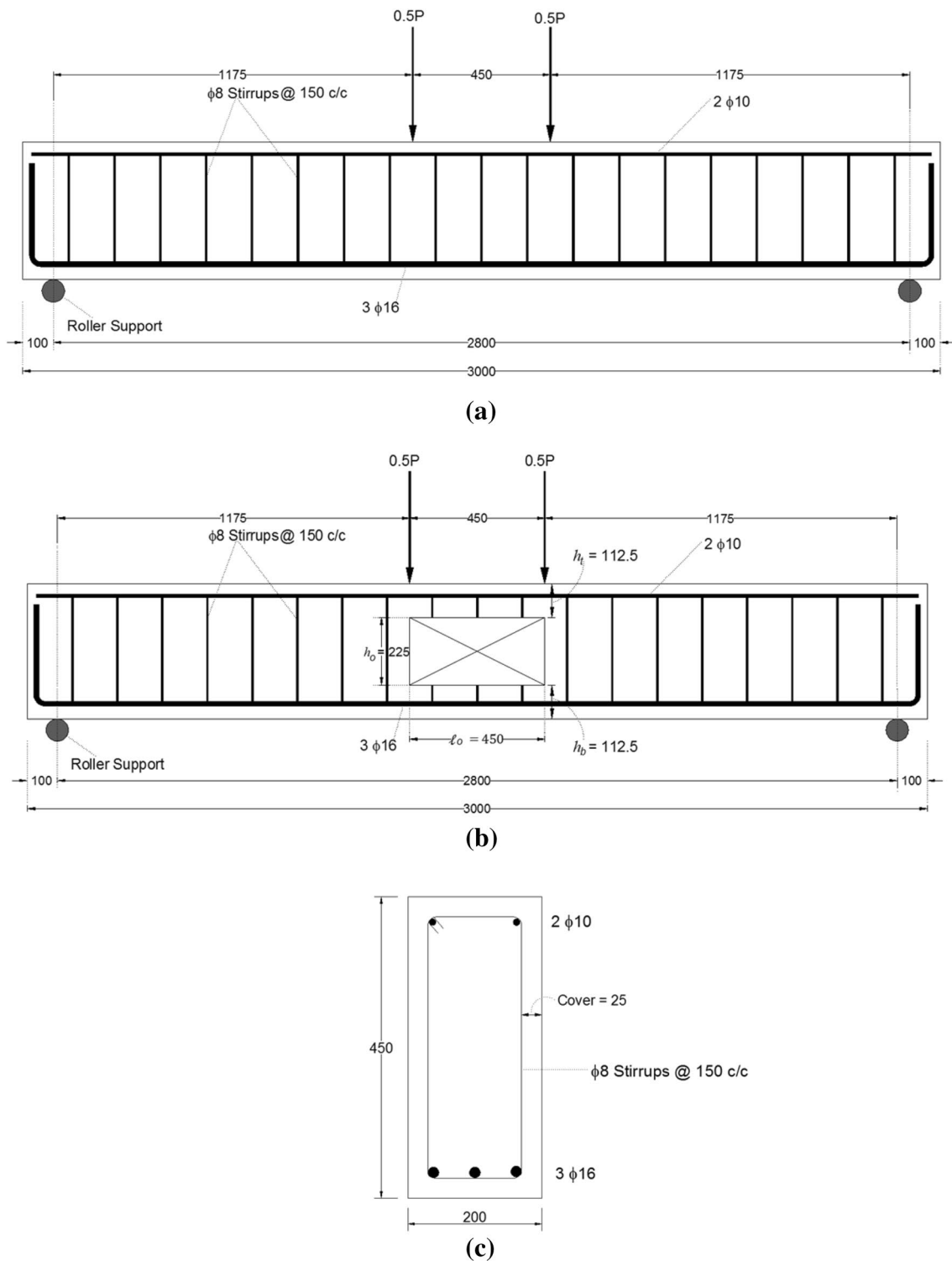


Fig. 2 Details of unstrengthened beams with 4-point bending (Note: all dimensions are in mm): **a** elevation of BC-N-4PB, **b** elevation of beam BC-O1-4PB, and **c** beam section.

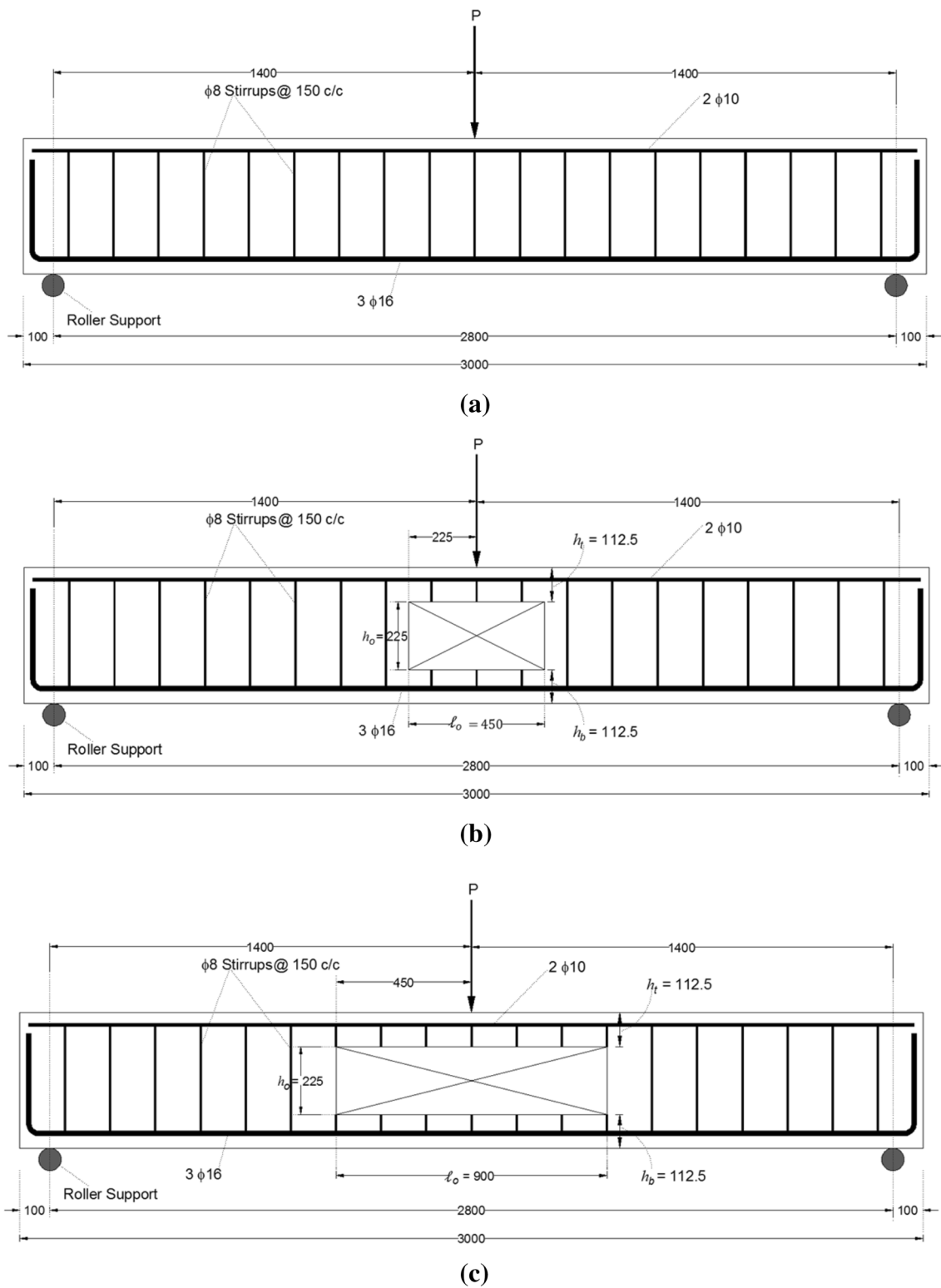


Fig. 3 Details of unstrengthened beams with center-point loading (Note: all dimensions are in mm): **a** elevation of beam BC-N-CPL, **b** elevation of beam BC-O1-CPL, and **c** elevation of beam BC-O2-CPL.

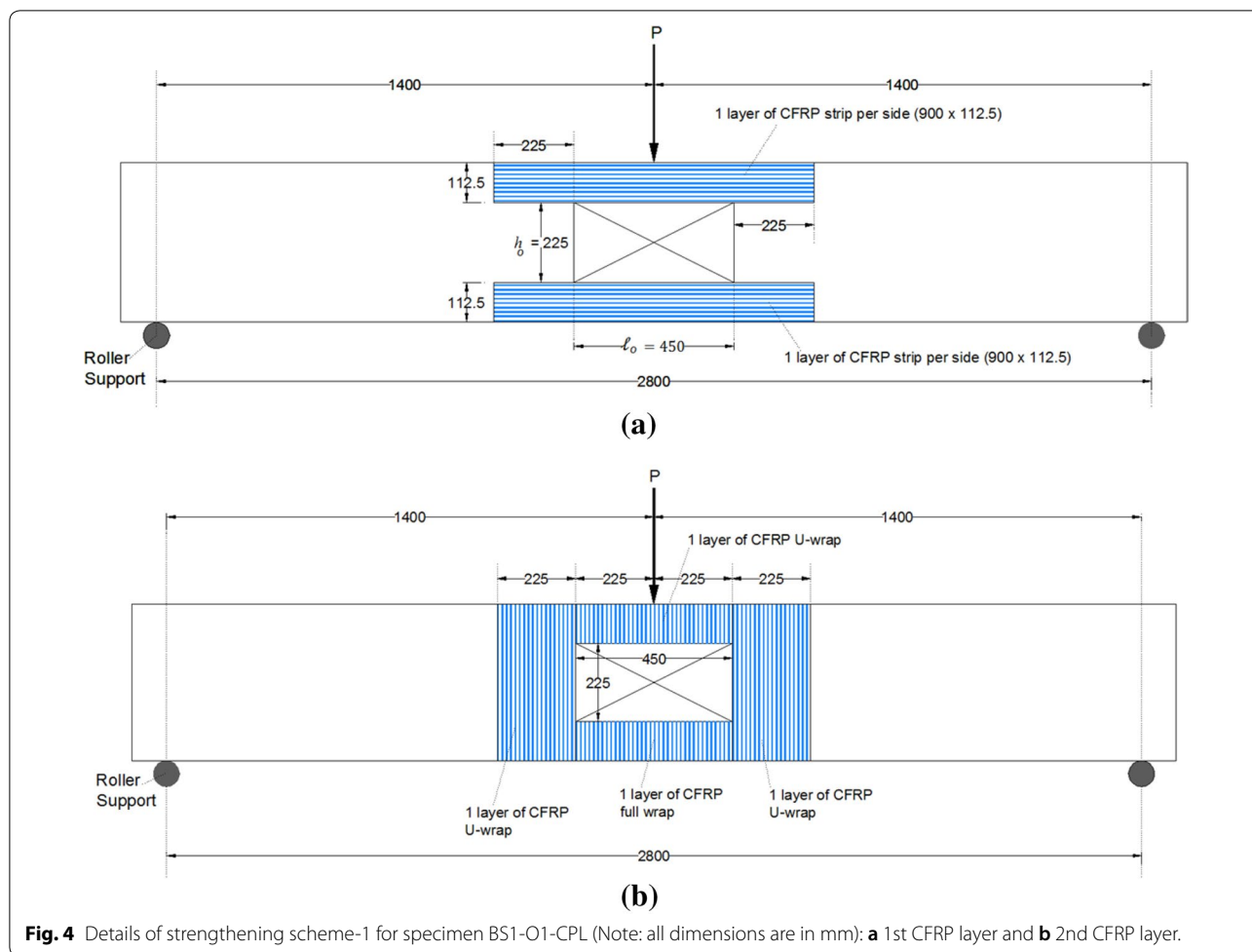


Fig. 4 Details of strengthening scheme-1 for specimen BS1-O1-CPL (Note: all dimensions are in mm): **a** 1st CFRP layer and **b** 2nd CFRP layer.

the same time add to the strength of the top chord. In this scheme, the reason for selecting GFRP instead of CFRP was to avoid the issue of galvanic corrosion, which arises as a result of metals connected to CFRP, so that this strengthening system could be used safely in the field. Details of beam BS2-O2-CPL strengthened with scheme-2 are given in Fig. 6. Furthermore, steps involved in strengthening of beam BS2-O2-CPL using scheme-2 are shown in Fig. 7. The layout of FRP sheets in the second scheme was essentially the same as scheme-1 with only one exception. The first layer of GFRP strips was not applied to the top chord on either side of the beam because of the presence of steel plates at this location. It was only applied to the bottom chord as seen in Fig. 6. The second layer of GFRP pattern was exactly the same as scheme-1 (Fig. 5). After the GFRP sheets were applied and the epoxy completely hardened, 5 mm thick ASTM A36 steel plates were bonded to the top chord of the beam as shown in Fig. 6. Holes were first driven at designated intervals in the concrete beam through the GFRP

sheet and 10 mm threaded rods (made of high-strength steel) passed through the holes. The space around the rods and concrete was completely closed with an epoxy adhesive mortar (Sika-41). Holes were then driven in the steel plates at the same location of the threaded rods in the beam. The steel plate was passed through the rods and bonded to the concrete surface. Epoxy adhesive mortar (Sika-41) was applied on the surface of the steel plate to fill in the gaps between the plate and the concrete. Pressure was applied until some of the epoxy squeezed out from in-between the steel plate and the GFRP-strengthened concrete surface. Nuts were then tightened on the 10 mm threaded rods thereby anchoring the steel plates to the GFRP-strengthened concrete surface strongly.

2.3 Material Properties

Ready-mix concrete was employed for casting the test specimens. The compressive strength of concrete on the test date, measured as per the ASTM C39/C39M

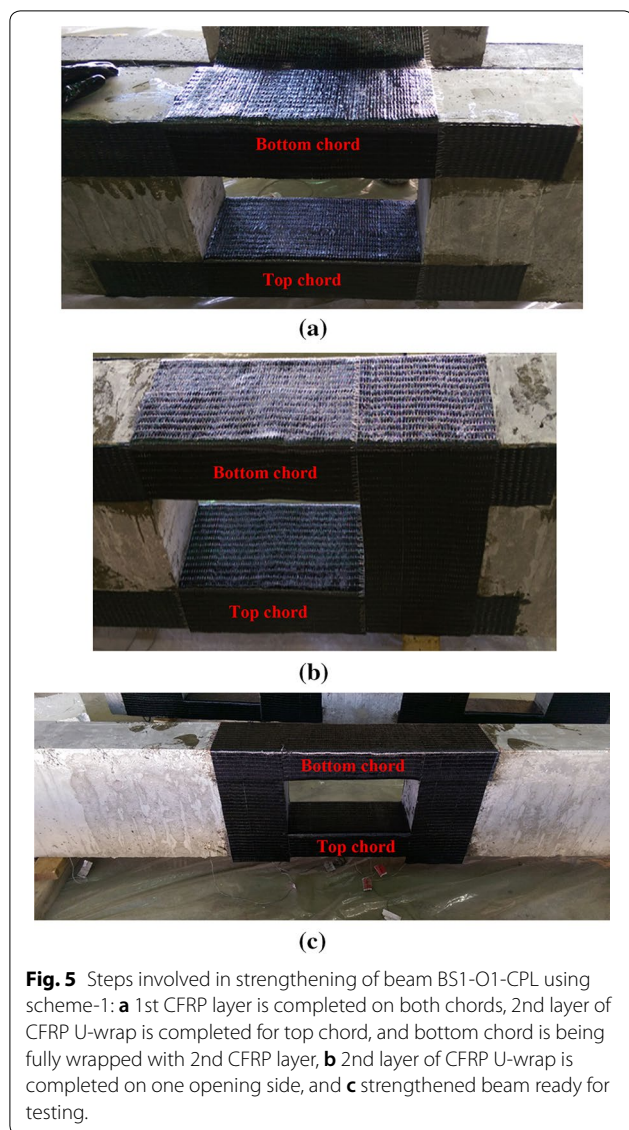


Fig. 5 Steps involved in strengthening of beam BS1-O1-CPL using scheme-1: **a** 1st CFRP layer is completed on both chords, 2nd layer of CFRP U-wrap is completed for top chord, and bottom chord is being fully wrapped with 2nd CFRP layer, **b** 2nd layer of CFRP U-wrap is completed on one opening side, and **c** strengthened beam ready for testing.

(2017), was 50 MPa. For steel rebars, direct tension tests were performed as per ASTM E8/E8M (2016) and the yield and tensile strengths of $\phi 8$, $\phi 10$ and $\phi 16$ mm rebars obtained from the tests are reported in Table 2. For steel plates, standard tension test coupons were cut, machined and then tested in accordance with ASTM A370 (2017) and the average value of the yield strength of plates is given in Table 2. The uni-directional CFRP and GFRP laminates were used in the study. Both strengthening systems of FRP were applied to the concrete surface using the conventional wet layup process. The standard coupons of CFRP and GFRP laminates were tested in tension as per ASTM D3039/3039M (2014) and the properties of the two laminates are reported in Table 2.

2.4 Instrumentation and Test Setup

Instrumentation layout and test setup for beams with center-point loading are shown in Fig. 8. As mentioned earlier, two beams (BC-N-4PB and BC-O1-4PB) were tested in four-point bending at a shear span of 1175 mm. However, the remaining five specimens were subjected to center-point loading thus giving a shear span of 1400 mm (see Fig. 8). The load was applied using a 2000-kN AMSLER testing machine. The load was recorded using a load cell, as shown in Fig. 8d. The test specimens were tested till failure under displacement control conditions at rate of 1 mm/min. The vertical deflections were recorded using linear variable displacement transducers (LVDTs) attached to the bottom of the beams. Moreover, strain gages were affixed to steel rebars at mid-span to record strains during the test (see Fig. 8a). Also, surface strain gages were affixed to FRP sheets and steel plates to measure their strains around the opening, as seen in Fig. 8b and c.

3 Discussion of Test Results

Table 3 shows a summary of test results of the seven specimens in terms of key parameters of load-deflection curves. It should be noted that the ultimate state used in Table 3 is defined as the state where the post-peak load drops to 80% of its peak value based on New Zealand Standard (1992). Table 4 displays measured peak strains for top and bottom rebars of the beam at mid-span and center of FRP layers and steel plate.

For the two beams with four-point bending, load versus deflection curves are plotted in Fig. 9a and the modes of failure are demonstrated in Fig. 10a and b. It is revealed that both beams BC-N-4PB and BC-O1-4PB had approximately the same behavior in terms of ultimate mode of failure and load-deflection characteristics, except that beam with opening (BC-O1-4PB) failed at an earlier stage with low ductility of 3.8 compared with 8.9 for solid beam BC-N-4PB. The two specimens showed nearly-bilinear response of under-reinforced concrete beams. The flexural failure of RC beams was initiated by yielding of main rebars. For solid beam BC-N-4PB, flexural cracks were developed at the mid-span and the mode of failure was due to concrete crushing (Fig. 10a). For beam BC-O1-4PB with opening and as a result of four-point bending setup, with two point loads applied at a distance of 450 mm from each other, the maximum bending moment was created within the section of the beam at the location of the opening. Failure of this beam was in flexure with cracks developing in tension zone and becoming wider as the load increased. Final failure was caused as a result of the top chord concrete crushing suddenly due

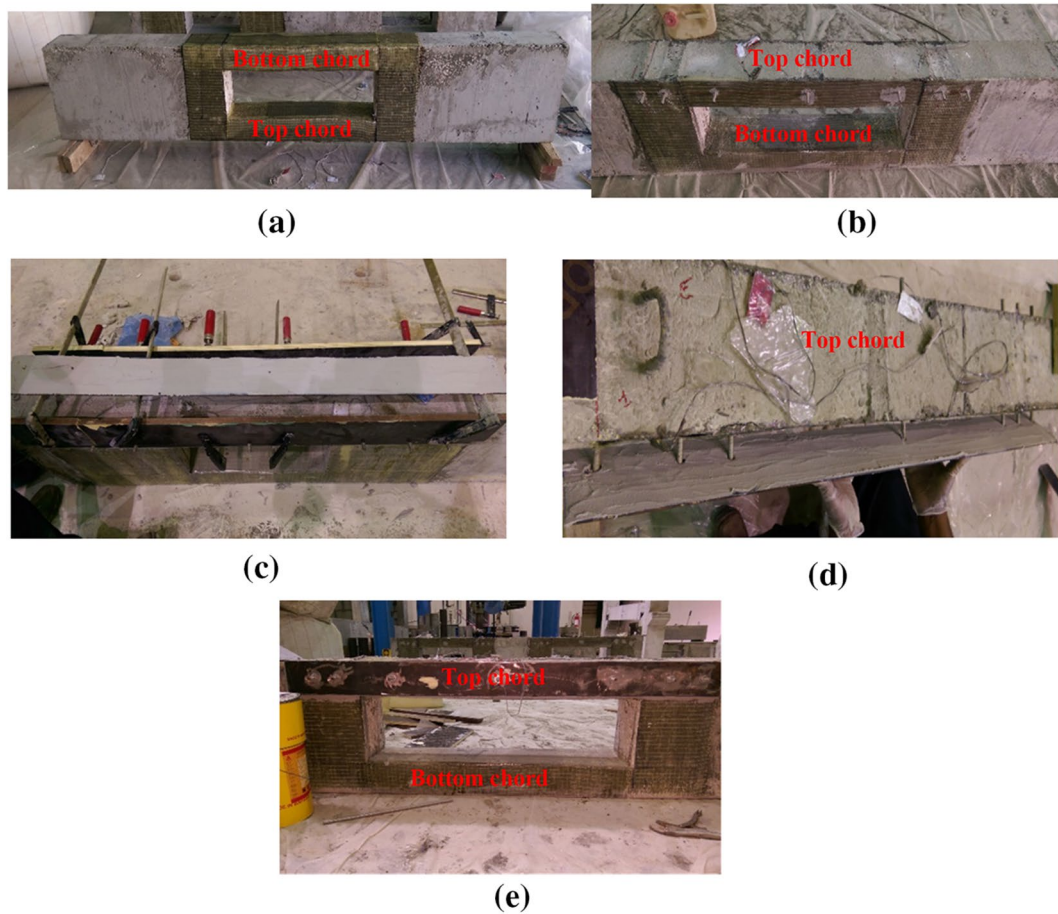


Fig. 7 Steps involved in strengthening of beam BS2-O2-CPL using scheme-2: **a** GFRP-strengthened beam, **b** holes drilled and threaded rods passed, **c** sika-41 epoxy applied to steel plates, **d** steel plates passed through the rods, and **e** strengthened beam ready for testing.

$$h_t \geq \frac{A_s f_y}{0.85 f'_c b} \tag{1}$$

where h_t is the depth of the top chord (Fig. 1), A_s is the area of longitudinal tension steel, f_y is the yield strength of longitudinal rebars, f'_c is the specified compressive strength of concrete, and b is the width of beam section.

For beams with center-point loading, load versus deflection curves are plotted in Fig. 9b and the final modes of failure are shown in Fig. 10c–g. As depicted from Fig. 10c, the final mode of failure of solid beam BC-N-CPL was similar to that of control beam BC-N-4PB tested under four-point bending. The beam failed in flexure with the yielding of longitudinal rebars leading to the crushing of concrete at the critical section. As seen from Fig. 9b, solid beam BC-N-CPL showed the nearly bilinear load-deflection response of under-reinforced concrete beams.

For control specimen BC-O1-CPL, with 450 mm opening and tested under center-point loading, the peak load was found to be 181 kN, which is about 83% of the ultimate load-carrying capacity of control solid beam BC-N-CPL. Because of the single point load applied at beam mid-span, both maximum shear as well as maximum moment were created within the section of the beam at the location of the opening. Noticed in this beam was a shear failure of the top chord, as seen in Fig. 10d. The failure was sudden and as a result, the beam exhibited brittle behavior with small mid-span deflection, as seen in Fig. 9b.

Figure 10e shows the final failure mode for the strengthened beam BS1-O1-CPL. A diagonal shear crack was observed propagating at a small distance from the loading point all the way to the edge of the opening thereby shearing the top chord. However, before the final failure, debonding of the second CFRP layer externally bonded to the top chord was noticed at the location of the major shear crack. There was no concrete adhering

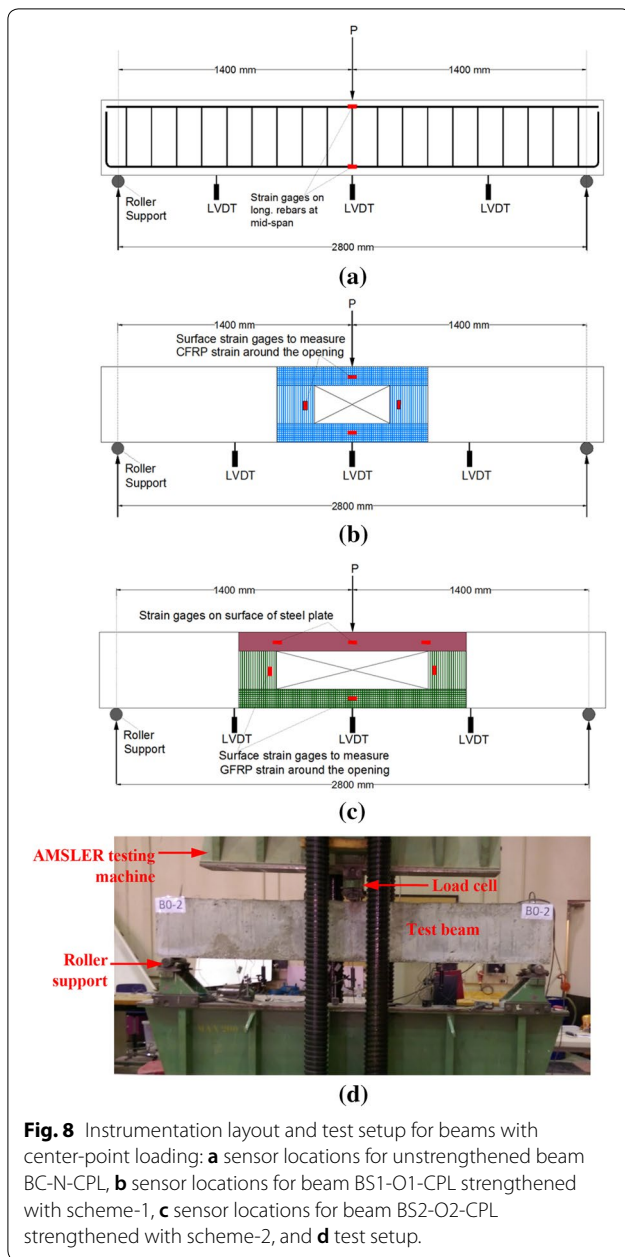
Table 2 Material properties used in the FE modeling.

Concrete					
Material model	Type 159 (MAT_CSCM_CONCRETE)				
Density (kg/m ³)	2320				
Uniaxial compressive strength (MPa)	50				
Max aggregate size (mm)	10				
Steel rebars, threaded rods and plates	ϕ8	ϕ10	ϕ16	Threaded rods	Plates
Material model	Type 24 (MAT_PIECEWISE_LINEAR_PLASTICITY)				
Density (kg/m ³)	7850				
Young's modulus (GPa)	200				
Poisson's ratio	0.3				
Yield stress (MPa)	570	575	575	350	250
Tangent modulus (MPa)	0	982	982	0	0
Plastic strain to failure (%)	11.7	11.7	11.7	19.8	19.9
FRP material	CFRP system				GFRP system
Material model	Type 54-55 (MAT_ENHANCED_COMPOSITE_DAMAGE)				
Density (kg/m ³)	1740				2550
Thickness per layer (mm)	1.0				1.3
Young's modulus in long. dir. (GPa)	82				20.9
Young's modulus in transverse dir. (GPa)	3.6				0.9
Longitudinal tensile strength (MPa)	834				460
Transverse tensile strength (MPa)	83.4				46

to the CFRP sheet. As seen from Fig. 10e, CFRP U-wrap for the entire top chord was found to be debonded from concrete. The peak load of the beam was 193 kN, which is only about 7% increase over that of unstrengthened specimen BC-O1-CPL. This load is about 89% of the peak load of control solid beam BC-N-CPL. This revealed the ineptitude of scheme-1 in increasing the load capacity of RC beams with opening located in the zone of high flexure with high shear.

For control unstrengthened beam with large mid-span opening of 900 mm and tested under center-point loading, the peak load was found to be 106 kN, which is considerably less compared to the control solid beam BC-N-CPL. This drop in the load is due to the larger size of the opening. The final failure was sudden because of shear cracking of the concrete in the top chord of the beam above the opening, as shown in Fig. 10f. A diagonal shear crack was noticed right under the loading point, which extended throughout the top-chord depth until the concrete section was completely sheared. Because of the large opening size, the top chord behaved as an independent beam supported between the two solid beam sections on either side of the opening. This had resulted in localized failure of the top chord with a small mid-span deflection of 3.5 mm at peak load, as seen in Fig. 9b.

As detailed earlier, scheme-2 involved using two layers of GFRP sheets along with steel plates for anchoring the GFRP sheets to the concrete surface. The anchorage system was devised as a way to combat debonding of the FRP sheets, which was observed in the failure mode of the beam strengthened with scheme-1. For beam BS2-O2-CPL with large opening and strengthened with scheme-2, the peak load was 201 kN, which is about 90% increase over that of unstrengthened specimen BC-O2-CPL. This load is also about 93% of the peak load of the control beam with no opening (BC-N-CPL). This shows the effectiveness of the strengthening system. The failure of this beam was due to out-of-plane buckling of steel plates close to the mid-span of the top chord followed by flexural failure of the top chord indicated by concrete crushing near the loading area (see Fig. 10g). Buckling of steel plates at the mid-point of the opening indicates their involvement in resisting load at that location. As seen in Fig. 9b, the mid-span deflection in the beam was small indicating local failure in the top chord as a result of the large size of the opening. Similar to specimen BC-O2-CPL, the top chord acted like an independent beam supported between the two solid beam sections on either side of the opening.



4 Finite Element Modeling

LS-DYNA (2007), a general-purpose FE software, was used for the numerical modeling of the RC beams. To account for the symmetry, only one-half of the test beam was modeled. The FE mesh of specimens BC-N-4PB (or BC-N-CPL) and BC-O1-4PB (or BC-O1-CPL) are shown in Fig. 11a and c, respectively. The concrete volume was represented by eight-node solid elements with single-point integration. The FE model of steel reinforcement for specimens BC-N-4PB (or BC-N-CPL) and BC-O1-4PB (or BC-O1-CPL) is displayed in Fig. 11b and d,

respectively. The steel rebars of RC beams were modeled using 2-node Hughes-Liu beam elements, whereas, 4-node Belytschko–Tsay shell elements (Belytschko and Tsay 1981) were used for modelling FRP laminates of strengthened specimens, as shown in Fig. 11e and f for beam BS1-O1-CPL. Eight-node reduced integration solid elements and 2-node Hughes-Liu beam elements, respectively, were used to model steel plates and threaded rods for beam BS2-O2-CPL, as seen in Fig. 11g. In the FE analysis, the bond between the steel rebars and the surrounding concrete and between the steel plates and the FRP laminates was assumed perfect.

The concrete volume was modeled using the continuous surface cap model type 159 of LS-DYNA (Murray 2007; Murray et al. 2007) along with the erosion option. The erosion of concrete elements was permitted when the principal strain in concrete exceeded 0.05 (Murray et al. 2007). The elasto-plastic material model type 24 was employed for modelling steel rebars, plates and threaded rods. In order to model the FRP laminates, the orthotropic material model type 54-55 was used with Chang and Chang failure criterion (Chang and Chang 1987). Table 2 provides the summary of the material properties employed in the non-linear FE analysis.

The bond between concrete and FRP laminates was represented using the tiebreak surface-to-surface contact type of LS-DYNA. Under the action of tensile and shear forces, the tiebreak permits the disengagement of the tied surfaces based on the bond strength failure criterion:

$$\left(\frac{|\sigma_n|}{NFLS}\right)^2 + \left(\frac{|\sigma_s|}{SFLS}\right)^2 \geq 1 \quad (2)$$

where σ_n and σ_s are the normal and shear stresses respectively, *NFLS* and *SFLS* are the normal and shear failure stresses respectively, which were estimated as follows (Chen and Teng 2001; Lu et al. 2005):

$$NFLS = 0.62\sqrt{f'_c} \text{ (MPa)} \quad (3)$$

$$SFLS = 1.5\beta_w NFLS \quad (4)$$

where β_w is a parameter given by

$$\beta_w = \sqrt{\frac{2.25 - b_f/b_c}{1.25 + b_f/b_c}} \quad (5)$$

where b_c and b_f are the width of RC beam and FRP laminates, respectively. This contact modeling approach has

Table 3 Comparison of experimental and FE load-deflection characteristics for test beams.

Beam ID	Results	P_y (kN)	P_u (kN)	Δ_y (mm)	Δ_u (mm)	K_s (kN/mm)	μ_Δ	E_u (kN·m)	Failure mode
BC-N-4PB	EXP	208	239	9.4	83.9	22.1	8.9	17,566	Y-CC
	FE	226	238	9.4	85.7	24.2	9.1	18,208	Y-CC
	EXP/FE	0.92	1.00	1.00	0.98	0.92	0.98	0.96	
BC-O1-4PB	EXP	215	244	8.9	34.2	24.2	3.8	6876	Y-CC
	FE	216	231	9.5	35.7	22.8	3.8	7179	Y-CC
	EXP/FE	0.99	1.05	0.94	0.96	1.06	1.02	0.96	
BC-N-CPL	EXP	180	217	7.5	76.9	24.0	10.3	15,283	Y-CC
	FE	178	204	7.0	85.0	25.3	12.1	16,358	Y-CC
	EXP/FE	1.01	1.06	1.07	0.90	0.95	0.85	0.93	
BC-O1-CPL	EXP	NY	181	NY	7.0	25.8	–	766	SF-TC
	FE	NY	172	NY	7.6	22.7	–	827	SF-TC
	EXP/FE	–	1.05	–	0.92	1.14	–	0.93	
BS1-O1-CPL	EXP	NY	193	NY	8.6	22.4	–	1001	DB-SF-TC
	FE	NY	185	NY	9.1	20.3	–	1039	DB-SF-TC
	EXP/FE	–	1.05	–	0.95	1.10	–	0.96	
BC-O2-CPL	EXP	NY	106	NY	3.5	30.2	–	181	SF-TC
	FE	NY	96	NY	3.9	25.0	–	211	SF-TC
	EXP/FE	–	1.10	–	0.91	1.21	–	0.86	
BS2-O2-CPL	EXP	NY	201	NY	6.4	31.4	–	788	BKL-FF-TC
	FE	NY	192	NY	5.7	33.8	–	637	BKL-FF-TC
	EXP/FE	–	1.05	–	1.13	0.93	–	1.24	

P_y and Δ_y load and mid-span deflection at yielding of bottom steel rebars, P_u ultimate load, Δ_u mid-span deflection at ultimate state, K_s effective pre-yield stiffness, μ_Δ deflection ductility ratio = Δ_u/Δ_y , E_u energy dissipated at ultimate state, Y-CC bottom steel yielding followed by concrete crushing at mid-span, SF-TC shear failure of top chord, DB-SF-TC FRP debonding followed by shear failure of top chord, BKL-FF-TC out-of-plane buckling of steel plates followed by flexural failure of top chord, EXP experimental, FE finite element, NY no steel yielding.

been validated earlier by the authors (Elsanadedy et al. 2013, 2015; Almusallam et al. 2015).

The roller support was represented by restricting the displacement of nodes in the global Z-direction (see Fig. 11). The nodes lying on the plane of symmetry were restrained against translation in the global X-direction and rotation about the global Y- and Z-directions. The displacement controlled loading was applied using a node set along the loading plane in order to control the Z-displacement during the test.

5 Validation of Finite Element Analysis

Test results of the seven specimens were employed for the validation of the numerical analysis and the modeling techniques. The results of the numerical study are discussed in the subsequent sub-sections.

5.1 Mode of Failure

Figure 12 shows the modes of failure for selected samples of test specimens, obtained using the post-processing software (LS-PrePost), at the end of the analysis time. The modes of failure in this figure are shown using contours of maximum principal strains at the mid-surface.

It is noticed from this figure that the failure modes observed in the numerical response match very well with the experiments. The numerical analysis revealed that the failure of control specimen BC-O1-4PB with 450 mm opening and tested under 4-point bending initiated with the formation of flexural cracks in the maximum-moment region and ultimately failed due to the crushing of concrete, as illustrated in Fig. 12a. For unstrengthened beams with openings and tested under center-point loading (BC-O1-CPL and BC-O2-CPL), sudden shear failure occurred in the top chord of the beam above the opening as seen in Fig. 12b and d. Figure 12c displays the FE mode of failure for strengthened beam BS1-O1-CPL. As seen from the figure, shear failure occurred in the top chord above the opening and it was preceded by debonding of the CFRP layer affixed to the top chord. Presented in Fig. 12e is the FE mode of failure for specimen BS2-O2-CPL with opening of 900 mm length and strengthened with scheme-2. Similar to the test results, failure of this beam was due to out-of-plane buckling of steel plates followed by flexural failure in the top chord above the opening.

Table 4 Comparison of experimental and FE peak strains for test beams.

Beam ID	Results	Strain in bottom rebars at mid-span ($\mu\epsilon$) ^a	Strain in top rebars at mid-span ($\mu\epsilon$) ^a	Strain in first FRP layer at mid-span ($\mu\epsilon$)		Strain in second FRP layer at mid-depth of opening edge ($\mu\epsilon$)	Mid-span steel plate strain at mid-depth of top chord ($\mu\epsilon$) ^a
				At mid-depth of bottom chord	At mid-depth of top chord		
BC-N-4PB	EXP	NA	- 14,841	-	-	-	-
	FE	69,540	- 14,036	-	-	-	-
	EXP/FE	-	1.06	-	-	-	-
BC-O1-4PB	EXP	26,705	- 7683	-	-	-	-
	FE	31,354	- 7797	-	-	-	-
	EXP/FE	0.85	0.99	-	-	-	-
BC-N-CPL	EXP	NA	- 5407	-	-	-	-
	FE	81,413	- 4980	-	-	-	-
	EXP/FE	-	1.09	-	-	-	-
BC-O1-CPL	EXP	2609	434	-	-	-	-
	FE	2583	460	-	-	-	-
	EXP/FE	1.01	0.94	-	-	-	-
BS1-O1-CPL	EXP	2549	350	2526	858	1931	-
	FE	2711	380	2771	691	2116	-
	EXP/FE	0.94	0.92	0.91	1.24	0.91	-
BC-O2-CPL	EXP	NA	19,297	-	-	-	-
	FE	1303	21,894	-	-	-	-
	EXP/FE	-	0.88	-	-	-	-
BS2-O2-CPL	EXP	1990	8995	1366	-	762	2807
	FE	2296	7768	1202	-	824	3033
	EXP/FE	0.87	1.16	1.14	-	0.92	0.93

Tensile strain is positive.

EXP experimental, FE finite element, NA not available data.

^a Values in italic bold font indicate steel yielding.

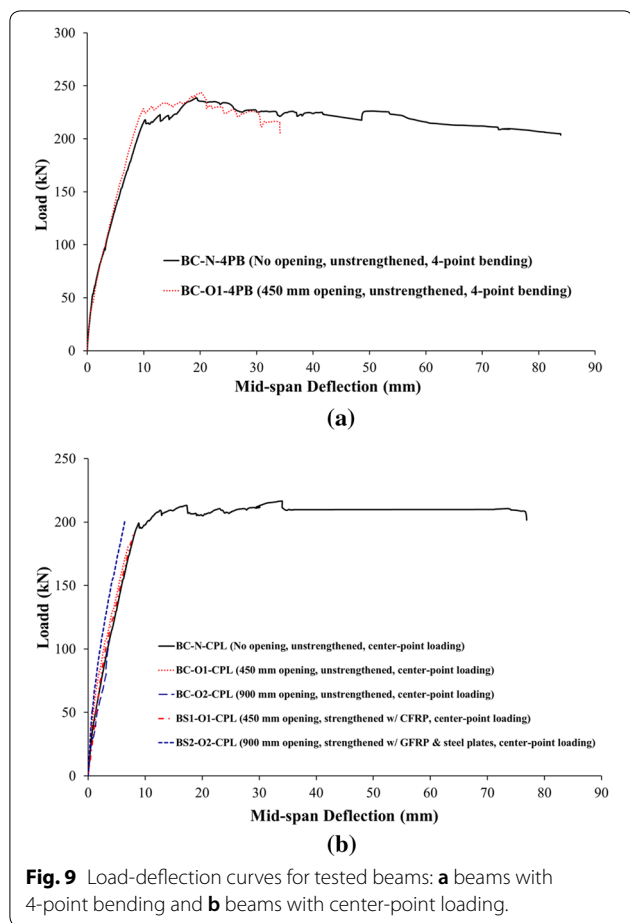
5.2 Load-Deflection Curves

Figure 13 depicts the plots of the experimental and numerical load versus mid-span deflection curves for the seven test specimens. A comparison between the experimental and numerical load-deflection curves illustrates good agreement. Table 3 enlists the comparison details in terms of load-deflection characteristics. As noted from Table 3, the deviations of 1–8 and 0–10% are observed for the numerical values of yield and peak loads, respectively. However, compared with the experimental results, deviations of 0–7 and 2–13% are observed for the mid-span deflections at yield and ultimate loads, respectively, whereas, the deviation in deflection ductility was 2–15%. The numerical prediction of effective stiffness of the test beams is also quite efficient with deviation ranging from 5 to 21%. As seen from Table 3, the energy dissipated (area under the load-deflection curve up to ultimate state) was predicted satisfactorily by the FE modeling with deviation ranging from 4 to 24%. The numerical analysis also illustrated the superiority of strengthening scheme-2 over scheme-1 in terms of improving the load-deflection

characteristics of RC beams with opening located in the zone of high flexure with high shear. Based on the results of numerical analysis, compared to the unstrengthened specimen with 900 mm opening, strengthening scheme-2 was successful in increasing the peak load by 100%. However, strengthening scheme-1 increased the peak load of unstrengthened beam with 450 mm opening by only 8%.

5.3 Strain Gage Results

Figures 14 and 15 show comparison curves of experimental and FE load versus strain of bottom and top rebars at mid-span of test beams, respectively. The figures show good match between the numerical and the experimental curves for all test specimens. Presented in Table 4 are measured and predicted peak strains for top and bottom rebars of beam at mid-span, mid-length of first FRP layer at mid-depth of top and bottom chords, second FRP layer at mid-depth of opening edge, and center of steel plate. The table shows that the prediction is conforming to the experiments. It is noted that for beams BC-N-4PB, BC-O1-4PB and BC-N-CPL, bottom and top



rebars at mid-span have yielded in tension and compression, respectively. For beams having 450 mm opening with center-point loading (BC-O1-CPL and BS1-O1-CPL), yielding was not noticed for either top or bottom rebars. For beams BC-O2-CPL and BS2-O2-CPL, as a result of the large opening size of 900 mm located in the zone of high flexure with high shear, the top chord behaved as an independent beam supported between the two solid beam sections on either side of the opening. Accordingly, as seen in Table 4 and Figs. 14 and 15, top steel rebars have yielded in tension; however, strains of bottom rebars were considerably below the yield strain. Table 4 evidences the insignificance of strengthening the bottom chord in case of large opening of 900 mm length. At mid-span of the bottom chord, horizontal FRP strain of about 6% of its rupture strain was noticed for beam BS2-O2-CPL, compared to strain of about 25% of FRP rupture strain at the same location for beam BS1-O1-CPL with 450 mm opening. Due to CFRP debonding at the top chord of beam BS1-O1-CPL, horizontal FRP strain of about 8% of CFRP rupture strain was observed in the top chord (Table 4). In conclusion, for beams with

center-point loading, load was shared between top and bottom chords in case of opening length of 450 mm; however, for large opening of 900 mm length, most of the load was taken by the top chord and the contribution of the bottom chord was minimal. This conclusion was also supported by strains of second FRP layer at mid-depth of opening edge. As seen in Table 4, very small value of about 3% of GFRP rupture strain was noticed in beam BS2-O2-CPL; however, strain of about 19% of CFRP rupture strain was observed in specimen BS1-O1-CPL. Table 4 also reveals the effectiveness of using steel plates in increasing the flexural and shear strength of the top chord of specimen BS2-O2-CPL as tensile strain of about 2.25 times the yield strain was noticed at mid-depth of steel plates. This demonstrated the full utilization of the yield capacity of the steel plates before buckling occurrence.

6 Parametric Study

6.1 Effect of Strengthening Scheme

Using simple elastic analysis calculations, the maximum pitch of threaded rods that could preclude elastic buckling of steel plates can be estimated from the following equation:

$$s_{max} = \pi t_p \sqrt{\frac{E_s}{12f_{yp}}} \tag{6}$$

where t_p thickness of steel plate; E_s Young’s modulus of steel = 2×10^5 MPa; and f_{yp} yield strength of steel plates. For the 5 mm thick steel plates used in this study, s_{max} was calculated to be 128 mm. However, as seen in Fig. 6, maximum spacing of 350 mm was used for specimens BS2-O2-CPL, which exceeded the 128 mm calculated from Eq. (6). Therefore, buckling occurred for plates of specimen BS2-O2-CPL. In brief, plate buckling could have been mitigated by the use of either lesser rod spacing (not exceeding 128 mm) or plates with larger thickness. The validated FE modeling was utilized to study the effect of steel plate parameters on performance of strengthened RC beams with web opening located in the zone of high flexure with high shear (case of center-point loading). In this regard, four new strengthening schemes (scheme-3 to scheme-6) were numerically investigated. Details of proposed schemes are shown in Figs. 16 and 17 for beams with 450 and 900 mm opening, respectively. It is clear that scheme-3 is the same as scheme-2 but with reduced rod spacing (maximum spacing of 125 mm was provided as seen in Figs. 16a and 17a). As depicted from Figs. 16b and 17b, strengthening scheme-4 is the same as scheme-2 but with larger plate thickness of 6.0 mm and reduced rod spacing (maximum spacing of 150 mm was

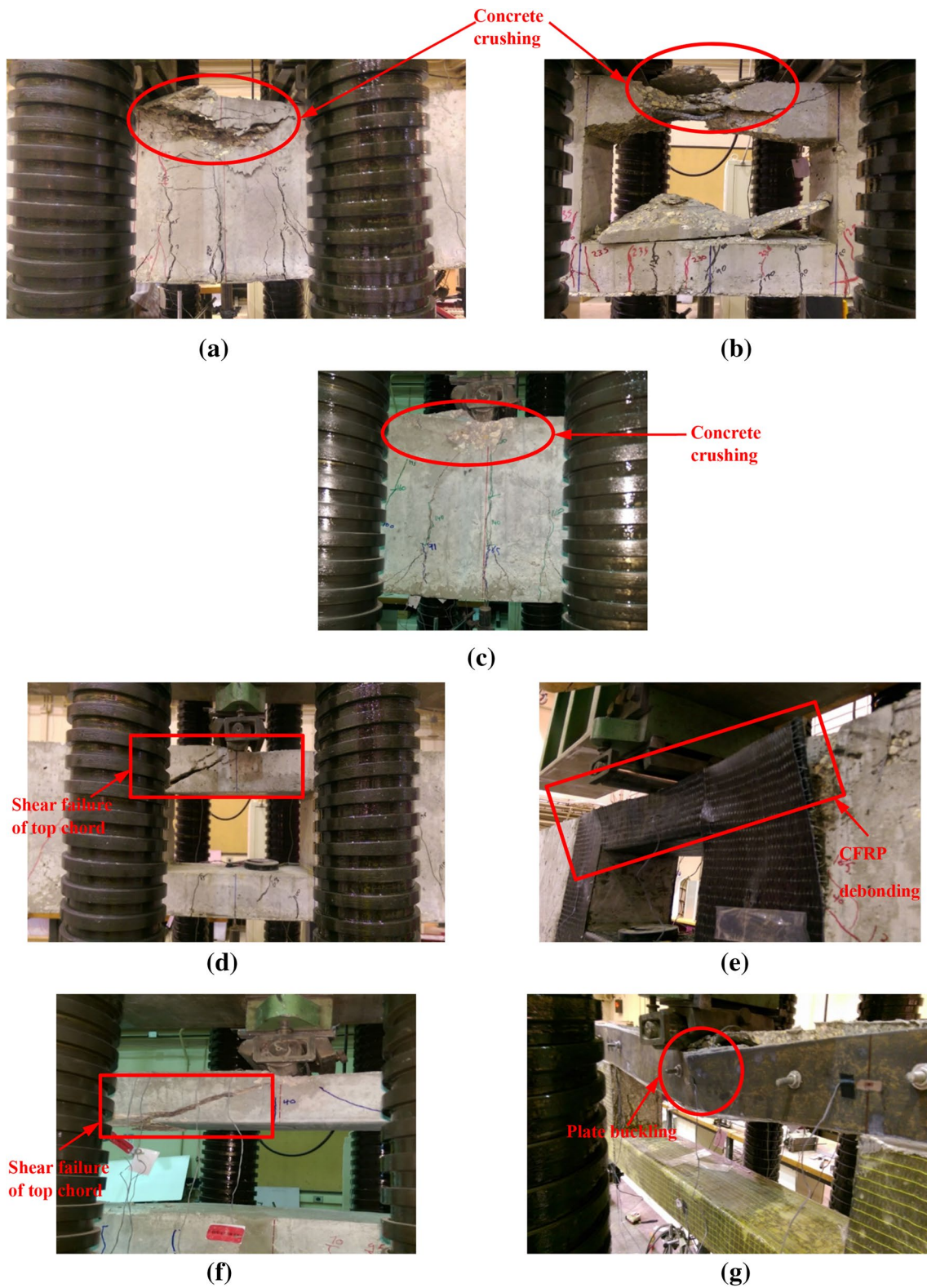


Fig. 10 Mode of failure for: **a** BC-N-4PB, **b** BC-O1-4PB, **c** BC-N-CPL, **d** BC-O1-CPL, **e** BS1-O1-CPL, **f** BC-O2-CPL, and **g** BS2-O2-CPL.

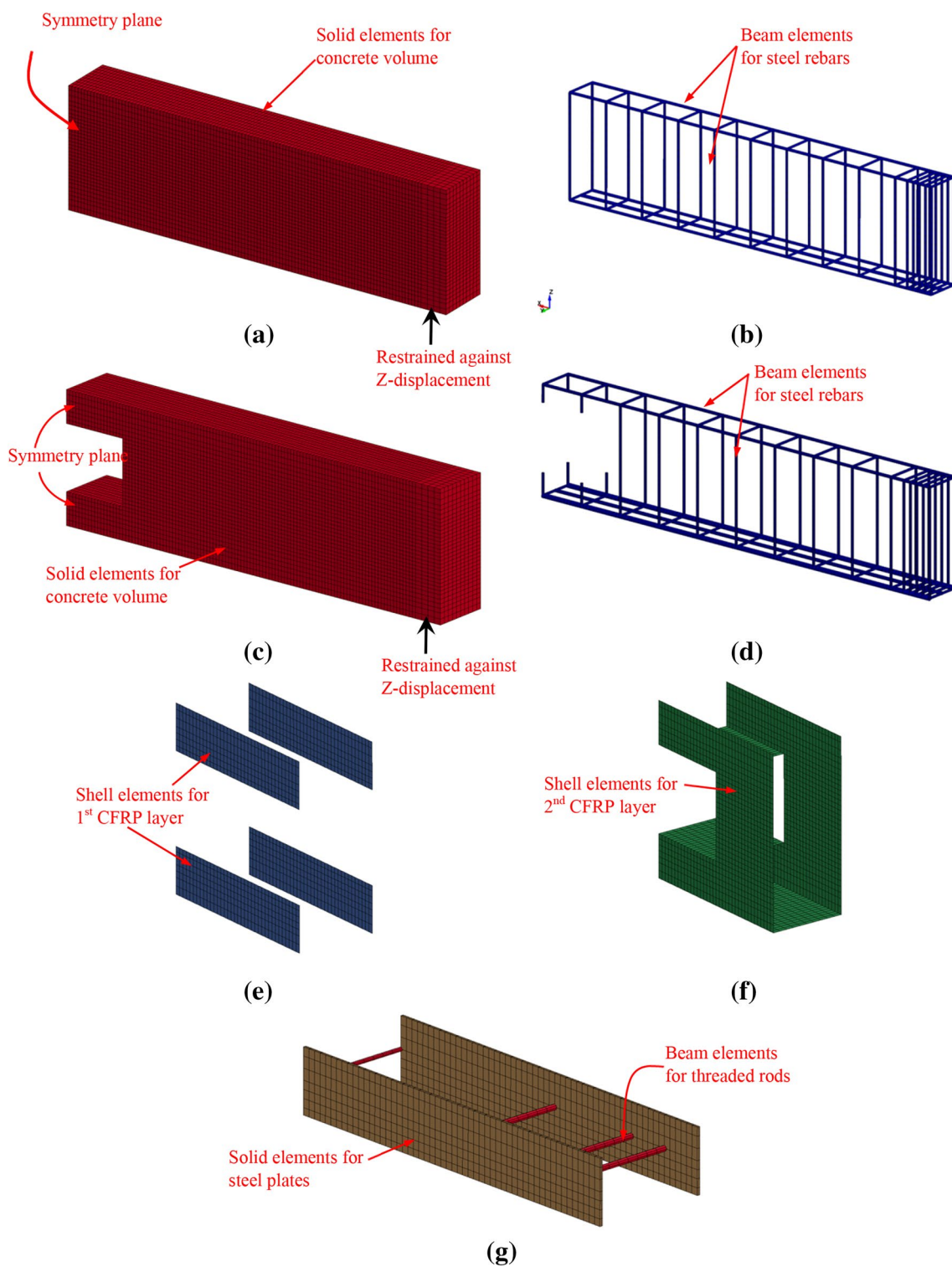


Fig. 11 FE model for one-half of specimens: **a** concrete volume for BC-N-4PB and BC-N-CPL, **b** steel rebars for BC-N-4PB and BC-N-CPL, **c** concrete volume for BC-O1-4PB and BC-O1-CPL, **d** steel rebars for BC-O1-4PB and BC-O1-CPL, **e** 1st CFRP layer for BS1-O1-CPL, **f** 2nd CFRP layer for BS1-O1-CPL, and **g** steel plates with rods for BS2-O2-CPL.

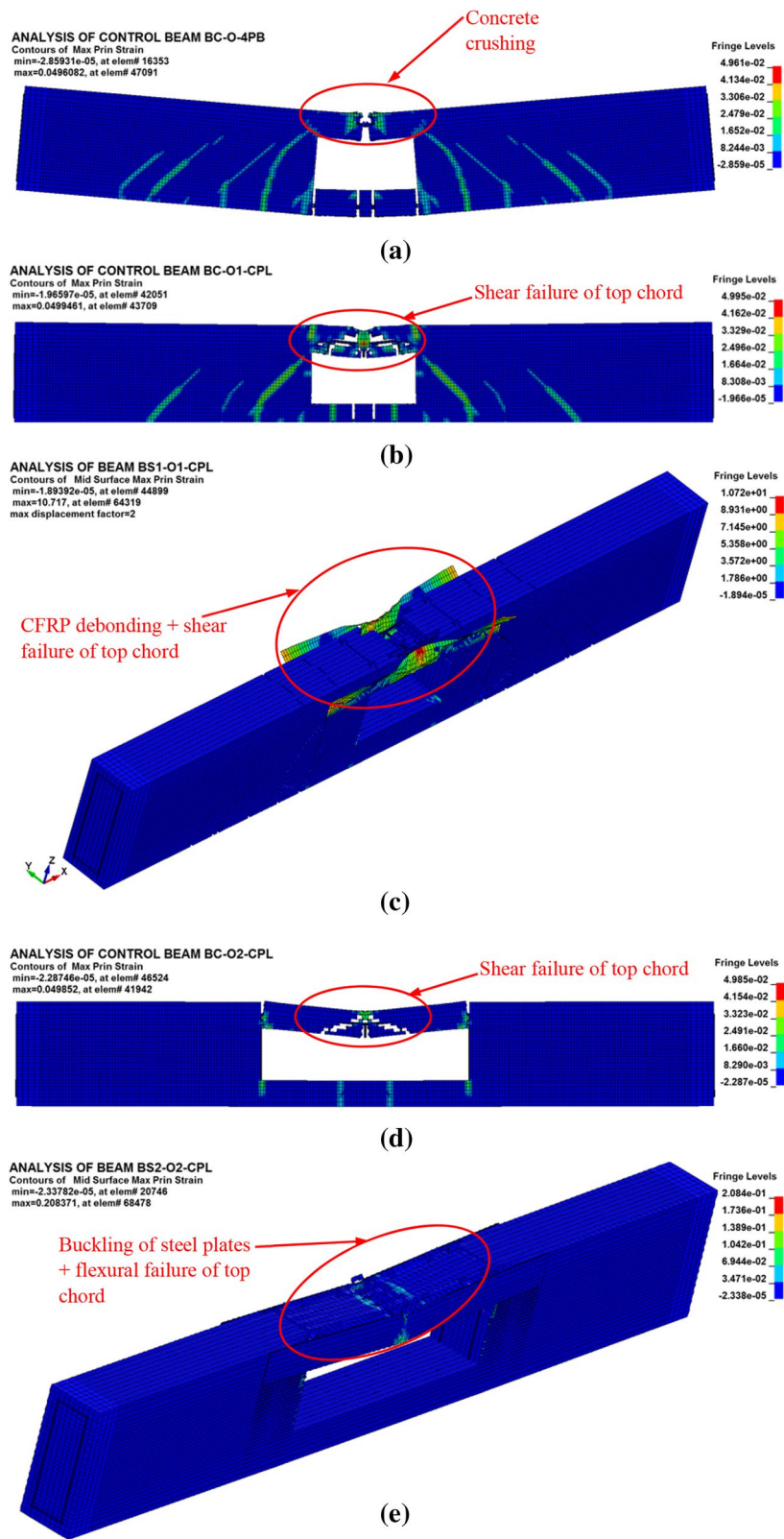


Fig. 12 FE modes of failure for: **a** BC-O1-4PB, **b** BC-O1-CPL, **c** BS1-O1-CPL, **d** BC-O2-CPL, and **e** BS2-O2-CPL.

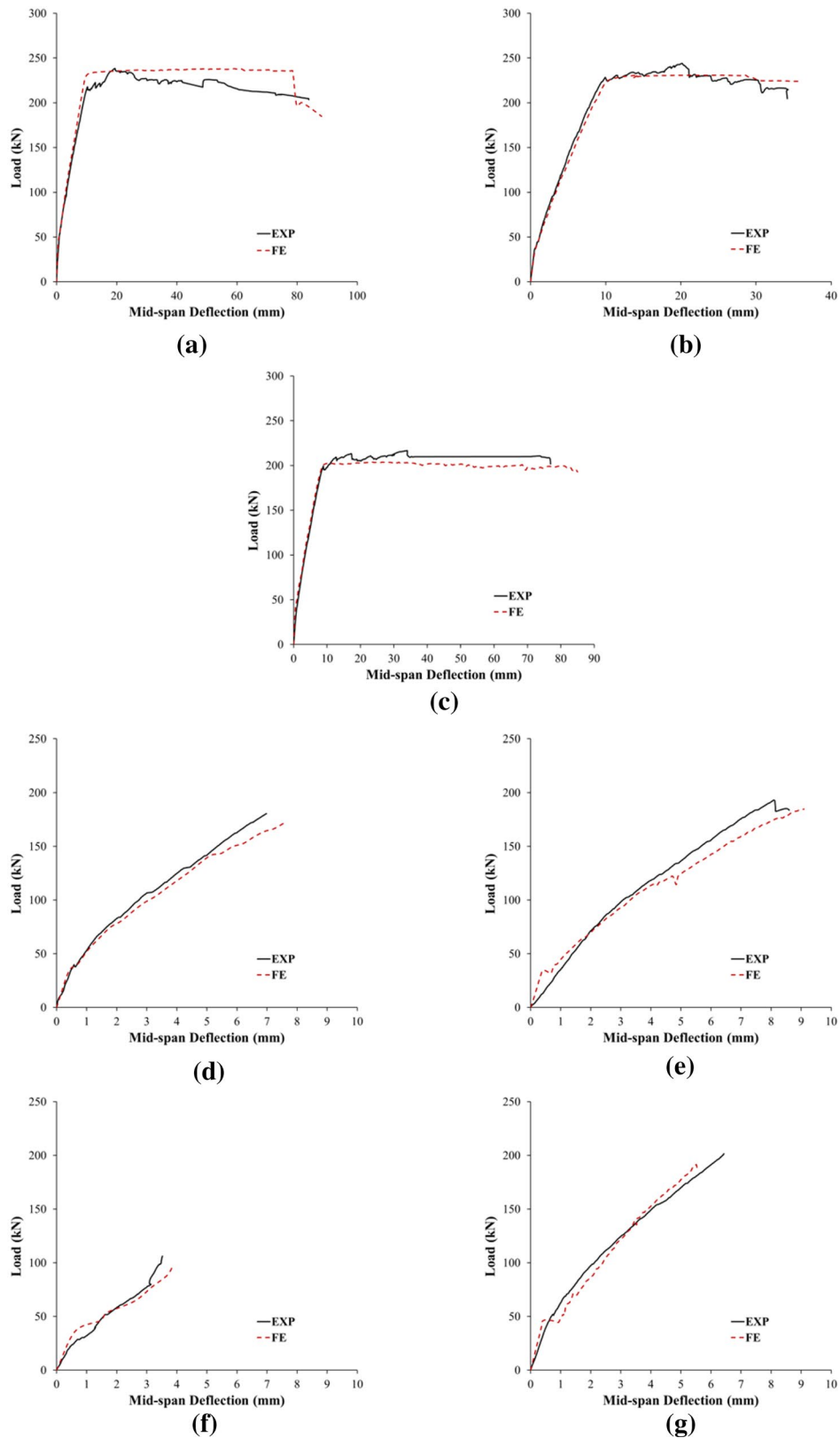


Fig. 13 Load-deflection comparison curves for: **a** BC-N-4PB, **b** BC-O1-4PB, **c** BC-N-CPL, **d** BC-O1-CPL, **e** BS1-O1-CPL, **f** BC-O2-CPL, and **g** BS2-O2-CPL.

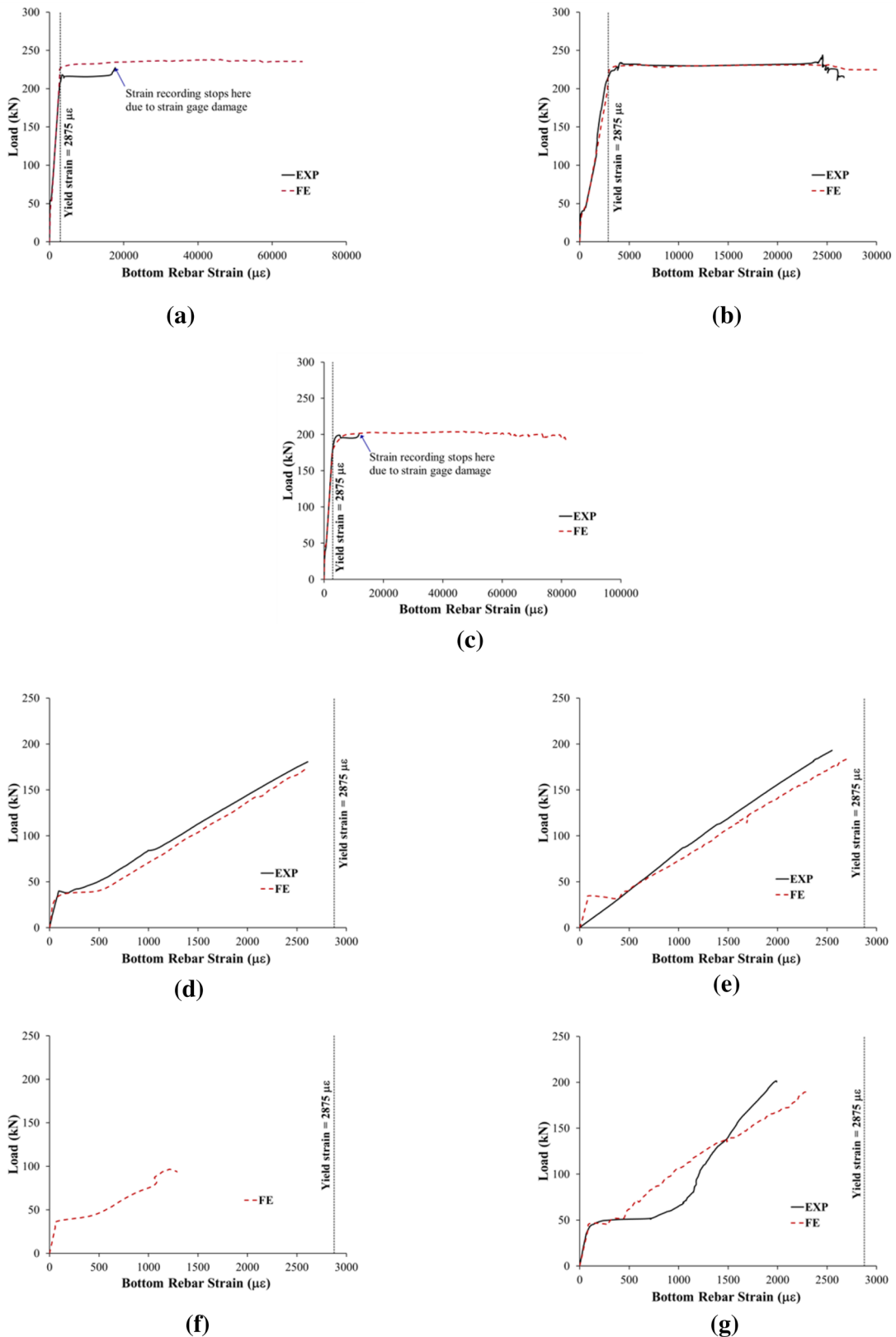


Fig. 14 Comparison curves of experimental and FE load versus strain of bottom rebars at mid-span of: **a** BC-N-4PB, **b** BC-O1-4PB, **c** BC-N-CPL, **d** BC-O1-CPL, **e** BS1-O1-CPL, **f** BC-O2-CPL, and **g** BS2-O2-CPL.

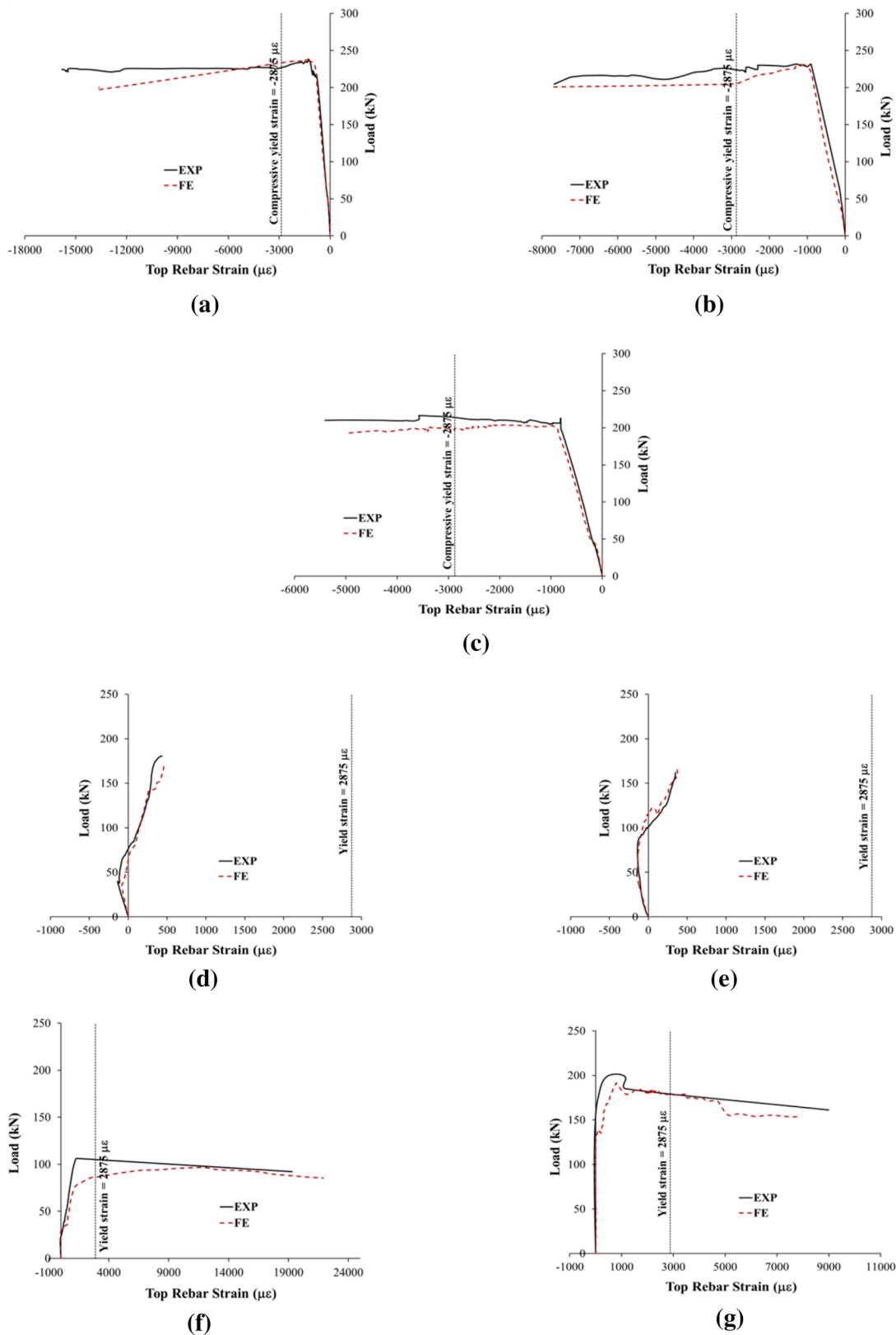


Fig. 15 Comparison curves of experimental and FE load versus strain of top rebars at mid-span of: **a** BC-N-4PB, **b** BC-O1-4PB, **c** BC-N-CPL, **d** BC-O1-CPL, **e** BS1-O1-CPL, **f** BC-O2-CPL, and **g** BS2-O2-CPL.

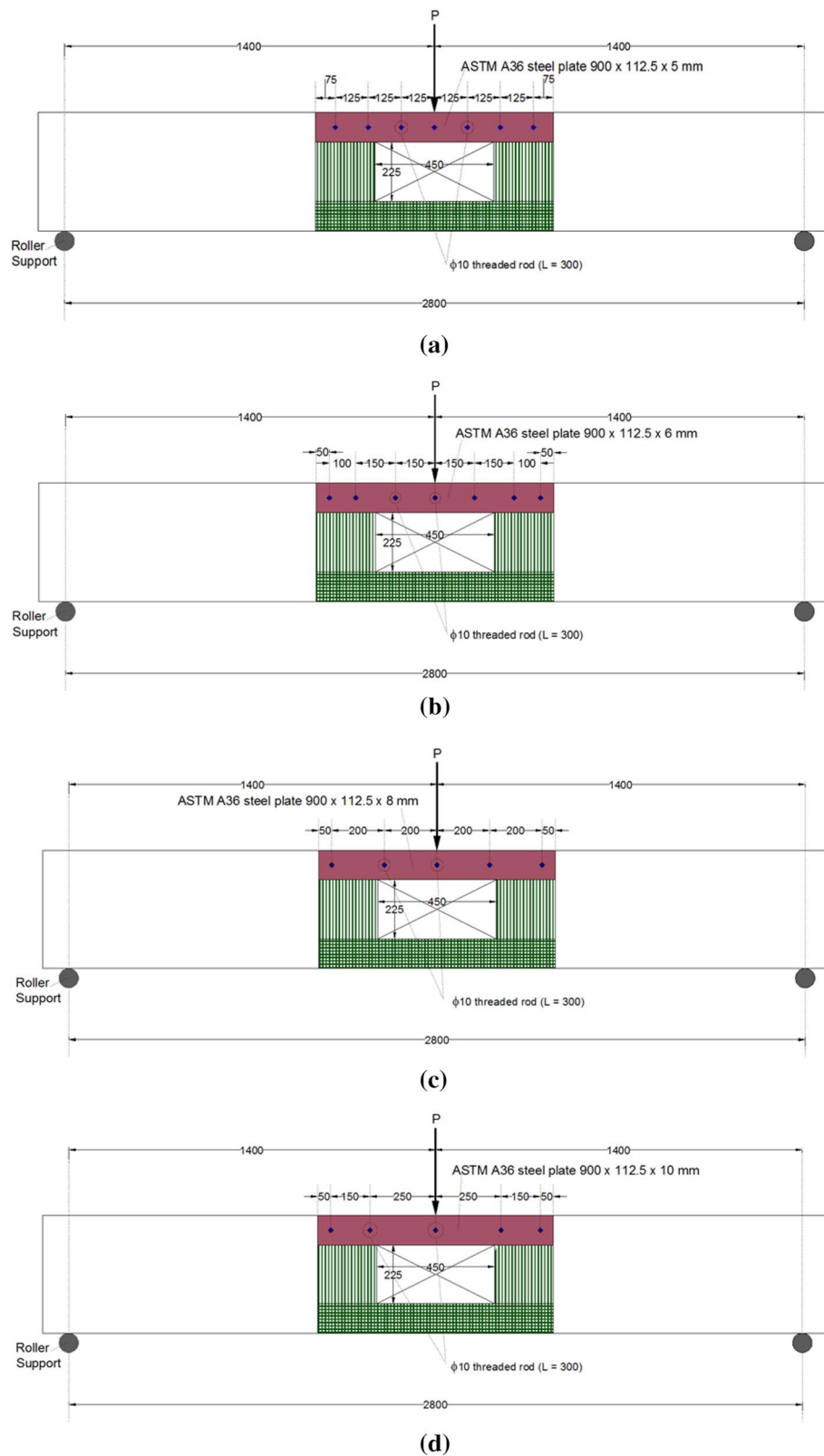


Fig. 16 Details of proposed strengthening schemes for beams with 450 mm opening (Note: all dimensions are in mm): **a** scheme-3, **b** scheme-4, **c** scheme-5, and **d** scheme-6.

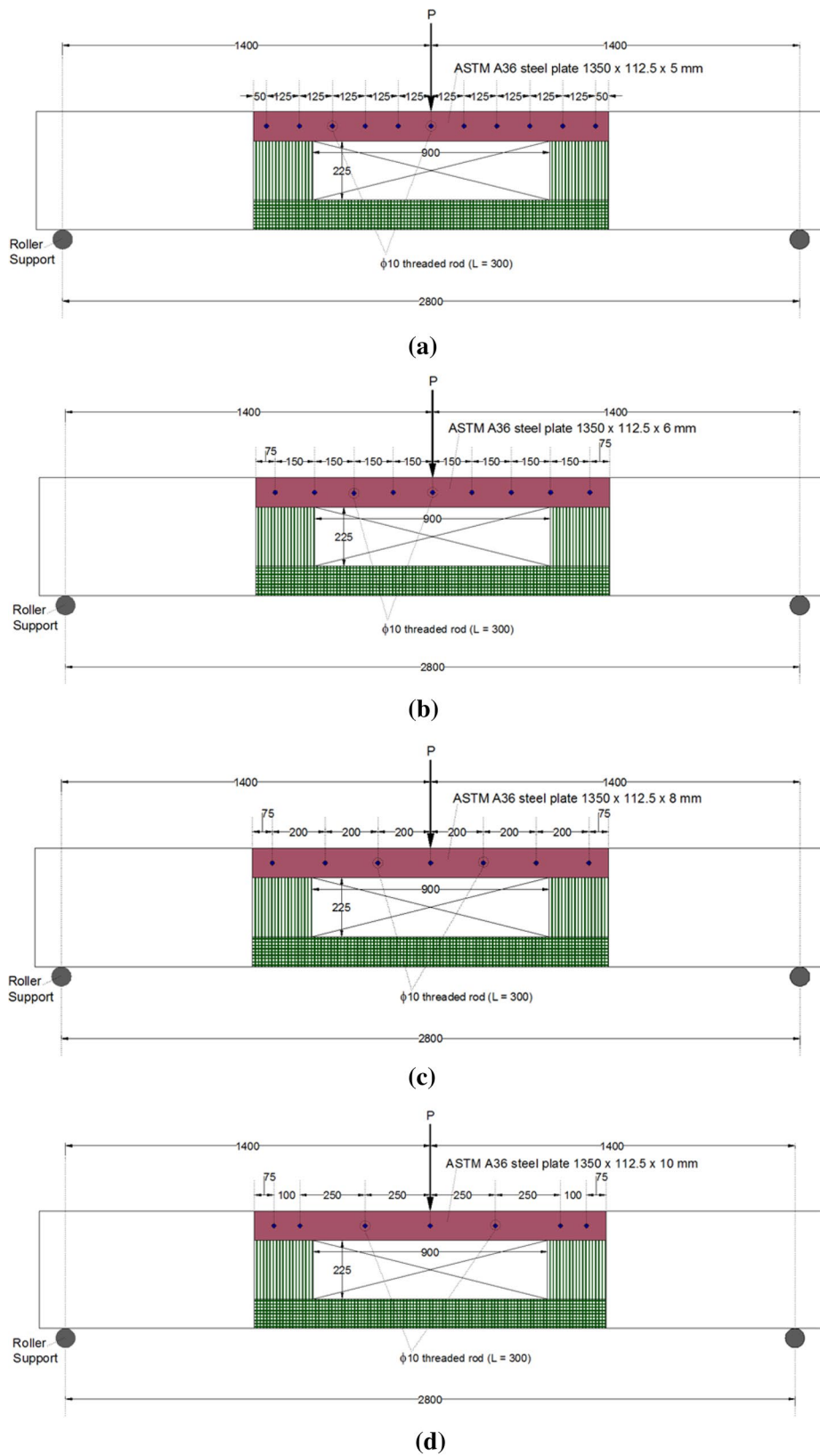


Fig. 17 Details of proposed strengthening schemes for beams with 900 mm opening (Note: all dimensions are in mm): **a** scheme-3, **b** scheme-4, **c** scheme-5, and **d** scheme-6.

Table 5 Details and FE results of beams used in the parametric study.

Beam ID	Opening size (mm)		ℓ_o/h_c	Type of loading	Strengthening scheme	FE results				
	h_o	ℓ_o				P_u (kN)	$\epsilon_{su,b}$ ($\mu\epsilon$)	$\epsilon_{su,t}$ ($\mu\epsilon$)	ϵ_{spu} ($\mu\epsilon$)	Failure mode
Effect of strengthening scheme										
BS1-O1-CPL	225	450	4.00	CPL	Scheme-1	185	2711	380	–	DB-SF-TC
BS3-O1-CPL	225	450	4.00	CPL	Scheme-3	236	11,620	468	–	FF-BM
BS4-O1-CPL	225	450	4.00	CPL	Scheme-4	239	12,285	477	15,657	FF-BM
BS5-O1-CPL	225	450	4.00	CPL	Scheme-5	239	11,530	710	9334	FF-BM
BS6-O1-CPL	225	450	4.00	CPL	Scheme-6	241	11,492	706	5203	FF-BM
BS2-O2-CPL	225	900	8.00	CPL	Scheme-2	192	2296	7768	43,317	BKL-FF-TC
BS3-O2-CPL	225	900	8.00	CPL	Scheme-3	201	2420	7989	49,394	FF-TC
BS4-O2-CPL	225	900	8.00	CPL	Scheme-4	204	2424	4464	48,903	FF-TC
BS5-O2-CPL	225	900	8.00	CPL	Scheme-5	209	2435	6429	33,688	FF-TC
BS6-O2-CPL	225	900	8.00	CPL	Scheme-6	214	2609	3781	30,634	FF-TC
Effect of opening size										
BU-0.0-CPL ^a	No opening		0	CPL	Unstrengthened	204	81,413	–4980	–	FF-BM
BU-1.0-CPL	225	113	1.00	CPL	Unstrengthened	203	55,071	2575	–	FF-BM
BU-2.0-CPL	225	225	2.00	CPL	Unstrengthened	200	39,071	2319	–	FF-BM
BU-3.0-CPL	225	338	3.00	CPL	Unstrengthened	198	24,286	2184	–	FF-BM
BU-4.0-CPL ^b	225	450	4.00	CPL	Unstrengthened	172	2583	460	–	SF-TC
BS4-4.0-CPL ^c	225	450	4.00	CPL	Scheme-4	239	12,285	477	15,657	FF-BM
BU-5.0-CPL	225	563	5.00	CPL	Unstrengthened	138	2040	689	–	SF-TC
BS4-5.0-CPL	225	563	5.00	CPL	Scheme-4	234	6444	852	18,523	FF-BM
BU-6.0-CPL	225	675	6.00	CPL	Unstrengthened	127	2006	12,855	–	SF-TC
BS4-6.0-CPL	225	675	6.00	CPL	Scheme-4	221	2881	1208	20,500	FF-BM
BU-8.0-CPL ^d	225	900	8.00	CPL	Unstrengthened	96	1303	21,894	–	SF-TC
BS4-8.0-CPL ^e	225	900	8.00	CPL	Scheme-4	204	2424	4464	48,903	FF-TC
BU-10.0-CPL	225	1125	10.00	CPL	Unstrengthened	54	755	27,289	–	FF-TC
BS4-10.0-CPL	225	1125	10.00	CPL	Scheme-4	169	1880	11,180	55,100	FF-TC
BU-12.0-CPL	225	1350	12.00	CPL	Unstrengthened	42	211	30,687	–	FF-TC
BS4-12.0-CPL	225	1350	12.00	CPL	Scheme-4	132	1388	13,344	62,224	FF-TC

h_o depth of opening, ℓ_o length of opening, h_c larger of h_b and h_t , where h_b and h_t = depth of bottom and top chords, respectively, P_u ultimate load, $\epsilon_{su,b}$ peak strain of bottom rebars at mid-span, $\epsilon_{su,t}$ peak strain of top rebars at mid-span, ϵ_{spu} peak tensile strain of steel plate at mid-span, *DB-SF-TC* FRP debonding followed by shear failure of top chord, *FF-BM* flexural failure of beam at opening with contribution from both top and bottom chords, *BKL-FF-TC* out-of-plane buckling of steel plates followed by flexural failure of top chord, *FF-TC* flexural failure of top chord, *SF-TC* shear failure of top chord, *CPL* Center-point loading.

^a Same as control beam BC-N-CPL.

^b Same as control beam BC-O1-CPL.

^c Same as beam BS4-O1-CPL.

^d Same as control beam BC-O2-CPL.

^e Same as beam BS4-O2-CPL.

used). In strengthening schemes 5 and 6, plate thickness was increased, respectively, to 8 mm and 10 mm and the rod spacing was, respectively, increased to 200 mm and 250 mm (see Figs. 16c, d, 17c and d). For beams having 450 mm opening, four new specimens (BS3-O1-CPL to BS6-O1-CPL) were added to the analysis matrix. For 900 mm opening, another four beams (BS3-O2-CPL to BS6-O2-CPL) were also numerically investigated. FE results of these eight specimens are listed in Table 5.

Presented in Fig. 18 is the effect of strengthening scheme on performance of beams with opening located in the zone of high flexure with high shear, based on FE analysis results. It is clear from Table 5 and Fig. 18a that for beams with 450 mm opening, strengthening schemes 3–6 gave almost same peak load and they were successful in altering the failure mode from sudden shear of top chord for unstrengthened beam to flexural failure at opening with contribution from both top and bottom

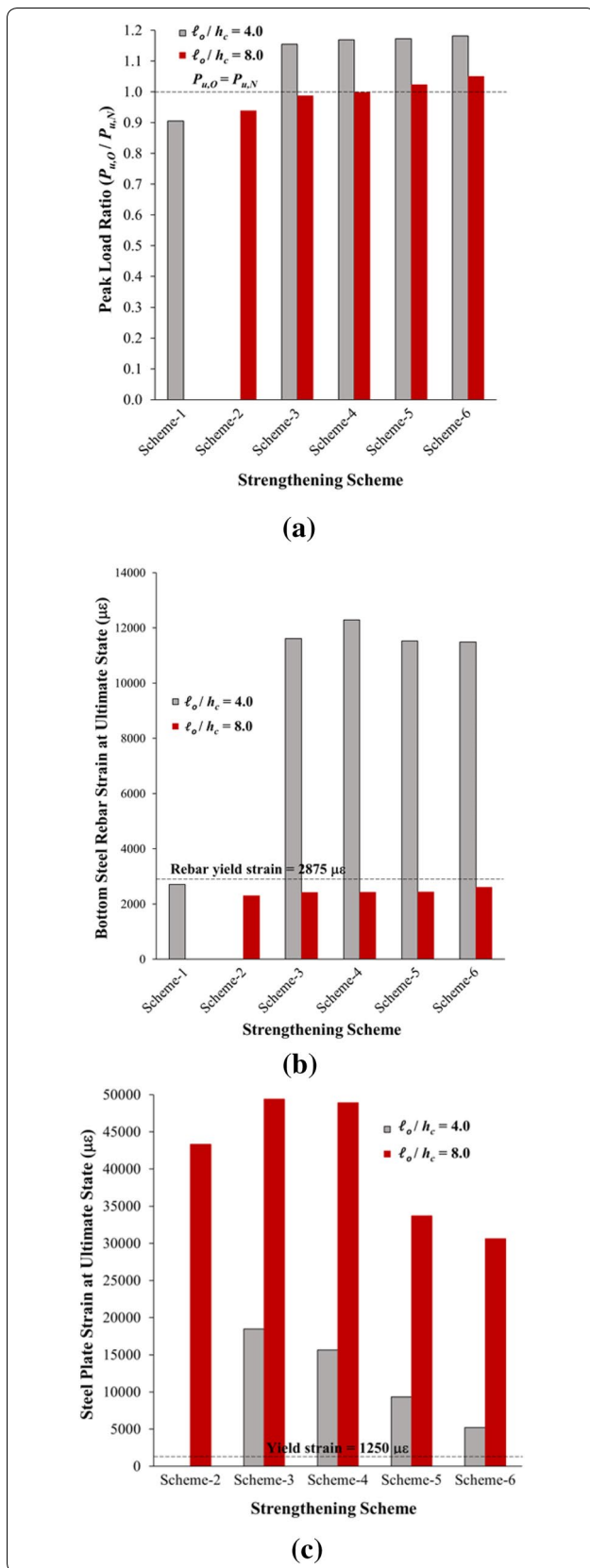


Fig. 18 Effect of strengthening scheme on performance of beams with openings and loaded at center point (based on FE analysis): **a** with respect to peak load, **b** with respect to strain of bottom steel rebars at mid-span, and **c** with respect to tensile strain of steel plate at mid-span.

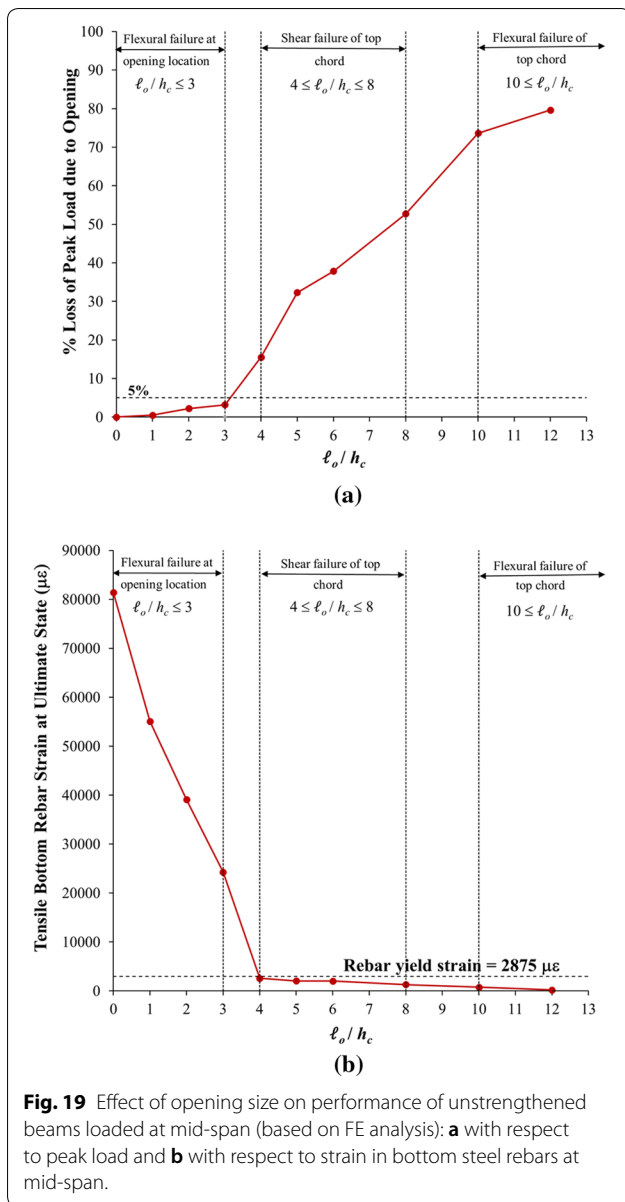
chords, as seen in Table 5. Strengthening schemes 3 to 6 were also effective in restoring the original beam capacity by giving peak load ratio (ratio of peak load of beam with opening, $P_{u,O}$ to peak load of solid beam, $P_{u,N}$) ranging from 1.15 to 1.18 as seen in Fig. 18a. It is also clear from Fig. 18b that large strains were predicted for bottom rebars at mid-span of beams strengthened with schemes 3–6, which confirms the contribution of the bottom chord in resisting the load for the case of 450 mm opening. In addition, as shown in Fig. 18c for 450 mm opening, large tensile strains were predicted at mid-length of steel plates of schemes 3–6 with the highest utilization of the plate strength for scheme-3, which has been reduced for schemes 4–6 due to the use of larger plate thicknesses.

For beams with 900 mm opening, it is demonstrated from Table 5 that strengthening schemes 3–6 changed the failure mode of unstrengthened specimen from brittle shear to flexural failure of the top chord. Table 5 and Fig. 18a also showed that schemes 4, 5 and 6 were able to at least restore the original beam capacity by having a peak load ratio ($P_{u,O}/P_{u,N}$) of 1.0, 1.02 and 1.05, respectively. As discussed earlier, because of the large opening size of 900 mm located in the zone of high flexure with high shear, the top chord behaved as an independent beam supported between the two solid beam sections on either side of the opening. Accordingly, as seen in Table 5, top steel rebars have yielded in tension; however, strains of bottom rebars were below the yield strain at beam mid-span (see Table 5 and Fig. 18b). As most of the load was taken by the top chord, very large strains were predicted for the steel plates of specimens BS3-O2-CPL and BS4-O2-CPL (see Table 5 and Fig. 18c), which have been reduced for schemes 5 and 6.

In conclusion, strengthening scheme-4 (with plate thickness of 6 mm and maximum rod spacing of 150 mm) was found to be the most economical scheme for both opening sizes as it was able to fully restore the original beam strength with the least plate thickness.

6.2 Effect of Opening Size

The validated FE modeling, detailed previously, was further extended to study the effect of different opening

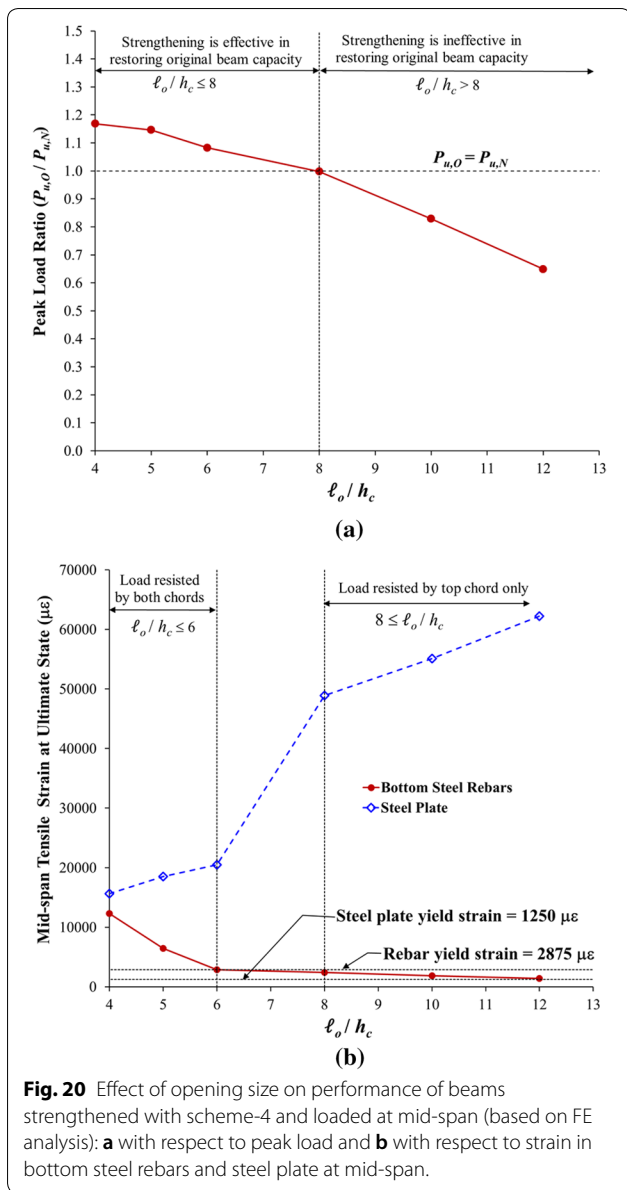


sizes on behavior of unstrengthened and strengthened beams with web opening located in the zone of high flexure with high shear (such as the case of center-point loading). Mansur and Tan (1999) suggested criteria for the selection of location of web openings in RC beams. The depth of openings was recommended not to exceed 50% of the overall depth of beam. Accordingly, in this study, the depth of the opening was not taken as a studied parameter and it was hence set equal to 225 mm. The length of the opening was taken as a studied parameter and it varied from zero (case of no opening) to 1350 mm. The maximum opening length of 1350 mm was chosen to have an opening extending approximately

to the mid-length of the shear span. Details of numerically investigated beams with different opening sizes are shown in Table 5. Ten opening lengths with ℓ_o/h_c (see Fig. 1) ranging from zero to 12 were numerically studied for unstrengthened beams. However, six opening lengths with ℓ_o/h_c ranging from 4 to 12 were numerically investigated for strengthened beams as seen in Table 5. Since scheme-4 was previously found to be the most economical scheme, it was used in this parametric study. The FE analysis results of beams with different opening sizes are listed in Table 5.

Figure 19 depicts the effect of opening size on performance of unstrengthened beams. As seen from Table 5 and Fig. 19, it is clear that as the opening size increased, peak load and tensile strain of bottom steel rebars at mid-span were reduced. As depicted from Fig. 19a and Table 5, flexural failure with yielding of main tension steel rebars was noticed for unstrengthened beams with $\ell_o/h_c \leq 3$. It is also clear from Fig. 19a that for unstrengthened specimens with $\ell_o/h_c \leq 3$, reduction in peak load due to opening was less than 5%, compared to solid beams (with no openings). In this case, strengthening may not be needed. For unstrengthened beams with $4 \leq \ell_o/h_c \leq 8$, failure was due to shear of the top chord with reduction in peak load due to opening ranging from 16 to 53%, as seen in Fig. 19a. However, for unstrengthened beams with $\ell_o/h_c \geq 10$, load was fully taken by the top chord and due to the large span-to-depth ratio of the top chord; flexural failure was predicted at critical sections of the top chord near mid-span and close to the opening edge. As seen in Fig. 19a, reduction in peak load due to opening ranged from 74 to 80% for beams with $\ell_o/h_c \geq 10$. Therefore, for unstrengthened beams with $\ell_o/h_c \geq 4$, strengthening is needed in order to fully or partially restore the original beam strength.

Figure 20 illustrates the effect of opening size on performance of beams strengthened with scheme-4 and loaded at center point, based on FE analysis. From Table 5 and Fig. 20a, it is demonstrated that for beams with $\ell_o/h_c \leq 8$, strengthening is effective at restoring the original beam strength with peak load ratio ($P_{u,O}/P_{u,N}$) ranging from 1.0 to 1.17. However, for beams with $\ell_o/h_c > 8$, strengthening could not fully restore the original beam strength and the peak load ratio ranged from 0.65 to 0.83, as seen in Fig. 20a. For beams with $\ell_o/h_c \leq 6$, load was resisted by both bottom and top chords. This is evident from Fig. 20b in which the bottom steel rebars at mid-span have yielded in tension for all beams with $\ell_o/h_c \leq 6$. However, for beams with $\ell_o/h_c \geq 8$, strains of bottom steel rebars were lower than the yield value and hence, most of the load was taken by the top chord. This was also confirmed from the high strain predicted for steel plates of beams with $\ell_o/h_c \geq 8$, as seen in Fig. 20b.



7 Conclusions

The following main conclusions can be drawn from this research:

- (1) The FE modeling used in this study was found appropriate in assessing the flexural strength of the unstrengthened as well as the FRP-strengthened RC beams with web openings in flexure zone. This demonstrates the validity of the modeling approach, which may be reliably used in future research on the use of FRP strengthening for RC structural members.

- (2) For RC beams with opening in the pure flexure zone, the ultimate capacity is not influenced by the opening if the depth of the top chord is more than or equal to the depth of the concrete stress block at ultimate state. Hence, strengthening is not required for such cases. However, in cases where the depth of the top chord is less than the depth of the concrete stress block, strengthening may be needed to restore the beam strength. A further study is strongly recommended to come up with the most effective strengthening scheme in such cases.
- (3) For RC beams with web openings located in the zone of high flexure with high shear (such as case of mid-span opening with center-point loading), reduction in strength due to opening is less than 5% when $l_o/h_c \leq 3$, where l_o is the length of the opening and h_c is the larger of h_b (depth of bottom chord) and h_t (depth of top chord). In this case, strengthening may not be needed. However, for beams with $4 \leq l_o/h_c \leq 8$, strengthening is required to restore the original beam strength. The proposed scheme-4 of this study (with steel plate thickness of 3% of the beam width and spacing between connecting rods less than the maximum pitch that could prevent elastic buckling of the steel plate) is recommended in this case. For beams with $l_o/h_c > 8$, strengthening may not be efficient to fully restore the original beam strength.

Authors' contributions

TA, YA-S and HE designed and wrote the manuscript; AA and RI reviewed and revised the manuscript. All authors read and approved the final manuscript.

Acknowledgements

The project was supported by Deanship of Scientific Research Chairs at King Saud University, Saudi Arabia for the Chair of Research and Studies in Strengthening and Rehabilitation of Structures at Civil Engineering Department.

Publisher's Note

Springer Nature remains neutral with regard to jurisdictional claims in published maps and institutional affiliations.

Received: 11 October 2017 Accepted: 16 April 2018

Published online: 26 July 2018

References

- Abdalla, H. A., Torkey, A. M., Haggag, H. A., & Abu-Amira, A. F. (2003). Design against cracking at openings in reinforced concrete beams strengthened with composite sheets. *Composite Structures*, 60(2), 197–204.
- Alagusundaramoorthy, P., Harik, I. E., & Choo, C. C. (2003). Flexural behavior of r/c beams strengthened with carbon fiber reinforced polymer sheets or fabric. *ASCE Journal of Composites for Construction*, 7(4), 292–301.
- Almusallam, T. H., Elsanadedy, H. M., & Al-Salloum, Y. A. (2015). Effect of longitudinal steel ratio on behavior of RC beams strengthened with

- FRP composites: Experimental and FE study. *Journal of Composites for Construction*, 19(1), 04014028.
- Al-Salloum, Y. A. (2007). Influence of edge sharpness on the strength of square concrete columns confined with composite laminates. *Composites Part B*, 38, 640–650.
- Al-Salloum, Y. A., Siddiqui, N. A., Elsanadedy, H. M., Abadel, A. A., & Aqel, M. A. (2011). Textile-reinforced mortar (TRM) versus FRP as strengthening material of seismically deficient RC beam-column joints. *ASCE Journal of Composites for Construction*, 15(6), 875–1002.
- Alsayed, S. H., Almusallam, T. H., Al-Salloum, Y. A., & Siddiqui, N. A. (2010). Seismic rehabilitation of corner RC beam-column joints using CFRP composites. *ASCE Journal of Composites for Construction*, 14(6), 681–692.
- Alsayed, S. H., Almusallam, T. H., Ibrahim, S. M., Al-Hazmi, N. M., Al-Salloum, Y. A., & Abbas, H. (2014). Experimental and numerical investigation for compression response of CFRP strengthened shape modified wall-like RC column. *Construction and Building Materials*, 63, 72–80.
- Ashour, A. F., El-Refaie, S. A., & Garrity, S. W. (2004). Flexural strengthening of RC continuous beams using CFRP laminates. *Cement and Concrete Composites*, 26(7), 765–775.
- ASTM. (2014). *Standard Test Method for Tensile Properties of Polymer Matrix Composite Materials*. ASTM D3039/D3039M—14, American Society for Testing and Materials, West Conshohocken, PA.
- ASTM. (2016). *Standard Test Methods for Tension Testing of Metallic Materials*. ASTM E8/E8M—16a, American Society for Testing and Materials, West Conshohocken, PA.
- ASTM. (2017). *Standard Test Method for Compressive Strength of Cylindrical Concrete Specimens*. ASTM C39/C39M—17, American Society for Testing and Materials, West Conshohocken, PA.
- ASTM. (2017). *Standard test Methods and Definitions for Mechanical Testing of Steel Products*. ASTM A370—17, American Society for Testing and Materials, West Conshohocken, PA.
- Belytschko, T. B., & Tsay, C. S. (1981). Explicit algorithms for non-linear dynamics of shells. *Journal of Applied Mechanical Engineering*, 48, 209–231.
- Chang, F. K., & Chang, K. Y. (1987). A progressive damage model for laminated composites containing stress concentration. *Journal of Composite Materials*, 21, 834–855.
- Chen, J. F., & Teng, J. G. (2001). Anchorage strength models for FRP and steel plates bonded to concrete. *Journal of Structural Engineering*, 127(7), 784–791.
- Chin, S., Shafiq, N., & Nuruddin, M. (2011). Strengthening of RC beams containing large opening at flexure with CFRP laminates. *World Academy of Science, Engineering and Technology, International Journal of Civil, Environmental, Structural, Construction and Architectural Engineering*, 5(12), 743–749.
- El Maaddawy, T., & Sherif, S. (2009). FRP composites for shear strengthening of reinforced concrete deep beams with openings. *Composite Structures*, 89, 60–69.
- Elsanadedy, H. M., Almusallam, T. H., Alsayed, S. H., & Al-Salloum, Y. A. (2013). Flexural strengthening of RC beams using textile reinforced mortar: Experimental and numerical study. *Composite Structures*, 97, 40–55.
- Elsanadedy, H. M., Almusallam, T. H., Alsayed, S. H., & Al-Salloum, Y. A. (2015). Experimental and FE study on RC one-way slabs upgraded with FRP composites. *KSCCE Journal of Civil Engineering*, 19(4), 1024–1040.
- Elsanadedy, H. M., Al-Salloum, Y. A., Abbas, H., & Alsayed, S. H. (2012a). Prediction of strength parameters of FRP confined concrete. *Composites Part B*, 43(2), 228–239.
- Elsanadedy, H. M., Al-Salloum, Y. A., Alsayed, S. H., & Iqbal, R. (2012b). Experimental and numerical investigation of size effects in FRP-wrapped concrete columns. *Construction and Building Materials*, 29, 56–72.
- Elsanadedy, H. M., Al-Salloum, Y. A., Al-Zaheri, Z. M., Alsayed, S. H., & Abbas, H. (2016). Behavior and design aspects of FRP-strengthened URM walls under out-of-plane loading. *ASCE Journal of Composites for Construction*, 20(6), 04016048.
- Hawileh, R., El-Maaddawy, T. A., & Naser, M. (2012). Non-linear finite element modeling of concrete deep beams with openings strengthened with externally-bonded composites. *Material Design*, 42, 378–387.
- Hawileh, R., Naser, M., & Abdalla, J. A. (2013). Finite element simulation of reinforced concrete beams externally strengthened with short-length CFRP plates. *Composites Part B*, 45(1), 1722–1730.
- Islam, M., Mansur, M. A., & Maalej, M. (2005). Shear strengthening of RC deep beams using externally bonded FRP systems. *Cement and Concrete Composites*, 27(3), 413–420.
- Kachlakev, D., & McCurry, D. D. (2000). Behavior of full-scale reinforced concrete beams retrofitted for shear and flexural with FRP laminates. *Composites Part B*, 31(6–7), 445–452.
- Li, A., Assih, J., & Yves, D. (2001). Shear strengthening of RC beams with externally bonded CFRP sheets. *Journal of Structural Engineering*, 127(4), 374–380.
- Livermore Software Technology Corporation (LSTC). (2007). *LS-DYNA User's Keyword Manual (Nonlinear Dynamic Analysis of Structures in Three Dimensions)*. Vol. 1. Version 971, LSTC, Livermore, CA.
- Lu, X. Z., Teng, J. G., Ye, L. P., & Jiang, J. J. (2005). Bond-slip models for sheets/plates bonded to concrete. *Engineering Structures*, 27(6), 920–937.
- Mansur, M. A. (1998). Effect of openings on the behavior and strength of R/C beams in shear. *Cement and Concrete Composites*, 20, 477–486.
- Mansur, M., & Tan, K. H. (1999). *Concrete beams with openings: Analysis and design*. Boca Raton: CRC Press.
- Mansur, M. A., Tan, K. H., & Wei, W. (1999). Effects of creating an opening in existing beams. *ACI Structural Journal*, 96(6), 899–906.
- Murray, Y. D. (2007). *User's Manual for LS-DYNA Concrete Material Model 159*. Report No. FHWA-HRT-05-062, US Department of Transportation, Federal Highway Administration National Transportation Systems Center, USA.
- Murray, Y. D., Abu-Odeh, A., Bligh, R. (2007). *Evaluation of Concrete Material Model 159*. Report No. FHWA-HRT-05-063, US Department of Transportation, Federal Highway Administration National Transportation Systems Center, USA.
- Nie, X. F., Zhang, S. S., Teng, J. G., & Chen, G. M. (2018). Experimental study on RC T-section beams with an FRP-strengthened web opening. *Composite Structures*, 185, 273–285.
- NZS 4203. (1992). New Zealand Standard, code of practice for general structural design and design loadings for buildings, p. 1.
- Pimanmas, A. (2010). Strengthening R/C beams with opening by externally installed FRP rods: Behavior and analysis. *Composite Structures*, 92, 1957–1976.
- Prentzas, E. G. (1968). *Behavior and Reinforcement of Concrete Beams with Large Rectangular Apertures*. Ph.D. Thesis, University of Sheffield, UK.
- Shehab, H. K., Eisa, A. S., & El-Awady, K. A. (2017). Strengthening of cutouts in existing one-way spanning R. C. flat slabs using CFRP sheets. *The International Journal of Concrete Structures and Materials*, 11(2), 327–341.
- Tan, K. H., Mansur, M. A., & Huang, L. (1996). Reinforced concrete T-beams with large web openings in positive and negative moment regions. *ACI Structural Journal*, 93(3), 277–289.
- Zhang, Z., Hsu, C., & Moren, J. (2004). Shear strengthening of reinforced concrete deep beams using carbon fiber reinforced polymer laminates. *Journal of Composites for Construction*, 8(5), 403–414.

Submit your manuscript to a SpringerOpen[®] journal and benefit from:

- Convenient online submission
- Rigorous peer review
- Open access: articles freely available online
- High visibility within the field
- Retaining the copyright to your article

Submit your next manuscript at ► [springeropen.com](https://www.springeropen.com)